DASY8/6 Modules WPT and SAR

APPLICATION NOTE

Testing for Compliance with FCC KDB 447498/680106(01/24)

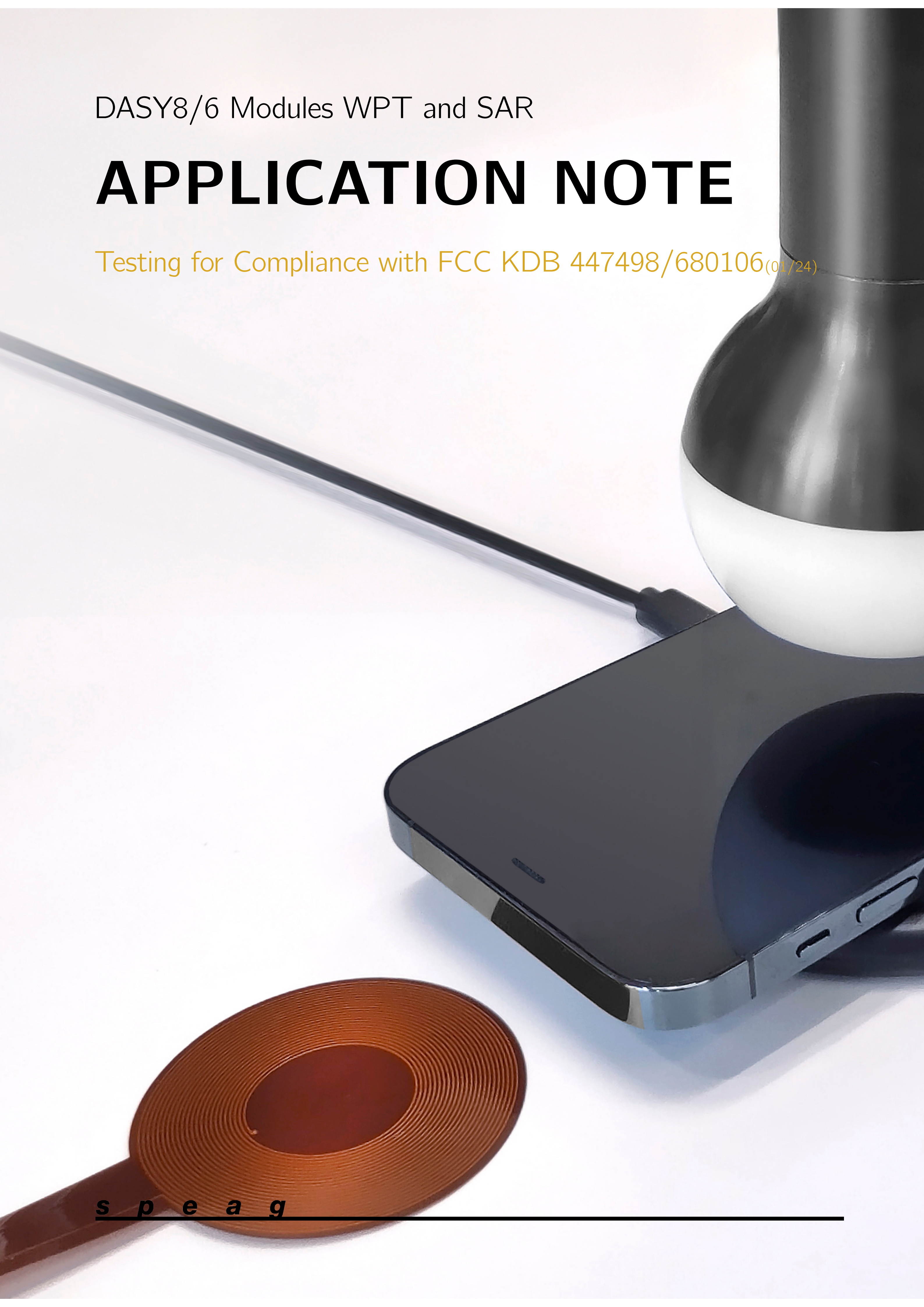

speag

Testing WPT Devices with DASY8/6 Modules WPT and SAR for Compliance with FCC KDB 447498/680106

1 Scope of this Document

This application note provides guidance on how to demonstrate compliance with specific absorption rate (SAR) limits in accordance with the US Federal Communications Commission (FCC) Knowledge Database (KDB) 447498 D01 [1] and FCC KDB 680106 D01 [2] for inductive wireless power transfer (WPT) devices[1] operating at frequencies ≥100 kHz and to assess compliance with the maximum permissible exposure (MPE) limits at frequencies <100 kHz.

2 FCC KDB 680106 D01 Exposure Assessment Requirements

2.1 Scope and Method

General radiofrequency (RF) exposure test requirements are described in FCC KDB 447498 D01 [1]. FCC KDB 680106 D01 [2] provides specific guidance for RF exposure compliance evaluations of WPT devices with respect to FCC equipment authorization for electromagnetic exposure.

The FCC has adopted SAR limits for RF exposure from 100 kHz to 6 GHz, as specified in §1.1310 of Title 47 of the US Code of Federal Regulations [3]. As an alternative to SAR, the guidelines described in [2] also permit evaluation of the incident electric (E-) and magnetic (H-) field strengths against the MPE limits summarized in Table 1 of KDB 447498 [4]. As stated in Section 3.2 of FCC KDB 680106 D01 [2]: *"In addition, present limitations of RF exposure evaluation systems prevent an accurate evaluation of SAR below 4 MHz. For these reasons, a specific MPE-based RF Exposure compliance procedure for devices operating in the aforementioned low-frequency ranges has been set in place."*

It is important to note that the FCC has not established limits to prevent nerve stimulation due to locally induced E-fields at frequencies below 10 MHz[2].

SPEAG has developed the technology to fill these gaps to enable evaluations of SAR, induced E-field, and incident fields from 3 kHz to 10 GHz and beyond.

Note: DASY8/6 Module WPT V2.4+ is the most accurate and versatile system for determination of SAR from 100 kHz to 4 MHz and the incident fields below 100 kHz for inductive WPT systems.

---

[1] This Application Note does not apply to radiative WPT devices and systems.

[2] Adoption of limits on induced E-field (in the frequency range 3 kHz to 10 MHz) at present remains under consideration in the open rulemaking proceeding FCC docket no. 19 226 (NPRM FCC-19-126) [5].

2.2 Compliance Testing Requirements

Section 3 of FCC KDB 680106 D01 [2] sets out the requirements for compliance testing of WPT devices.

Section 3.1 of KDB 680106 D01 defines the output power, separation distance, and use-case requirements, including justifications for the chosen minimum separation distance for specific use cases.

Section 3.2 of KDB 680106 D01 defines the requirements for situations where SAR cannot be measured and extends the MPE limits to frequencies below 300 kHz. For operating frequencies between 100 kHz and 300 kHz, the values at 300 kHz – i.e., E_{inc} = 614 V/m, H_{inc} = 1.63 A/m, which are root-mean-square (rms) values – apply[3]. For operating frequencies below 100 kHz, MPE limits are temporal peak values[4] of E_{inc} = 83 V/m, H_{inc} = 90 A/m (see Figures 1.1 and 1.2). Section 3.2 of KDB 680106 D01 exempts incident E-field measurements from the compliance testing for devices under test (DUTs) that operate at low frequencies (typically below 1 MHz) and use coil-type emitting structures that have H-fields as the dominant near field.

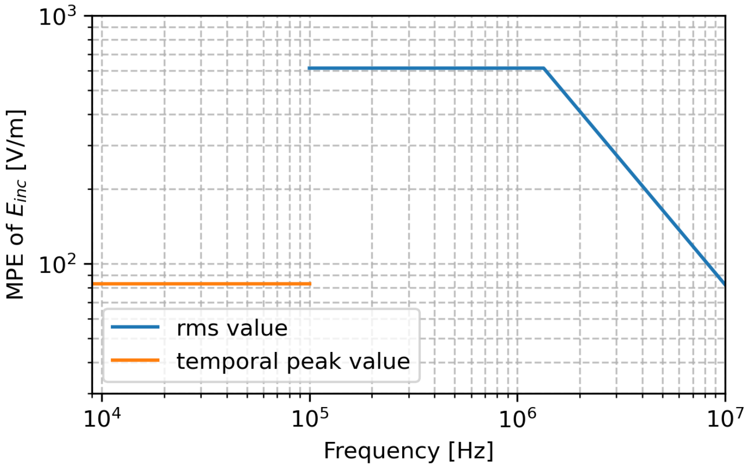

Figure 1.1: MPE limits of the incident E-field defined by the FCC. Note that the limits at frequencies ≥100 kHz are defined in terms of the rms value, while those at <100 kHz are defined in terms of the temporal peak value.

Section 3.3 of KDB 680106 D01 describes the requirements for measurement validation when probes with a greater than 5 mm sensor offset (i.e., the spacing between the sensor center and the probe outer surface) are used. The fields at positions that cannot be reached must be estimated via either a numerical calculation or an analytical model. The FCC also requests validation of the estimate by comparing the model prediction and the measurement result at the closest reachable positions. For a successful validation, the agreement should be better than 30%. As described in Section 6 of the DASY8/6 Module WPT Manual [6], the uncertainty of the surface field reconstruction of DASY8/6 Module WPT V2.4+ is well below this 30% requirement.

Section 4 of FCC KDB 680106 D01 provides guidance for the setup of instrumentation to test compliance of WPT devices that are co-located with other RF devices. The principle is that a WPT transmitter should be tested in the presence of a WPT receiver, given that the receiver structure can alter the field strength patterns.

---

[3] For § 2.1091 mobile devices and § 2.1093 portable devices intended for use by consumers in the general population / uncontrolled environments, only “source-based” time averaging per an inherent property of the RF source is permitted for determining exposure levels (6 min and 30 min time averaging provisions of § 1.1310, based on device maximum duty factor, are not applicable to consumer devices).

[4] Consistent with considerations in FCC-19-126 [5], transient or very short-term peak fields are taken as instantaneous values not to be time-averaged. These limits are applicable in uncontrolled exposure situations; higher limits might be acceptable in controlled exposure situations but require a KDB Inquiry.

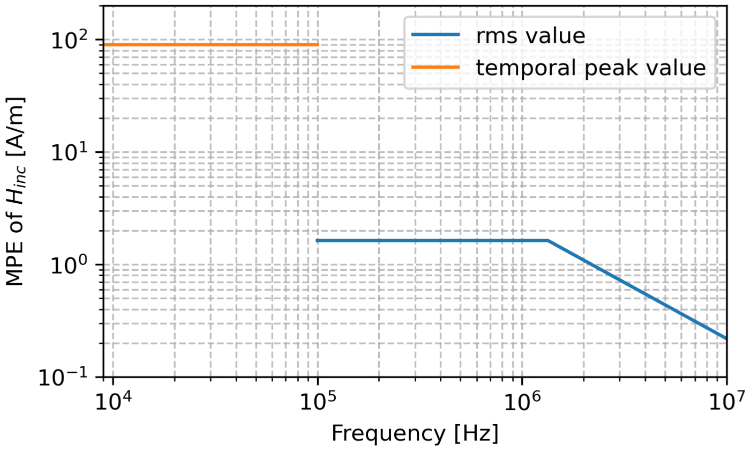

Figure 1.2: MPE limits of the incident H-field defined by the FCC. Note that the limits at frequencies ≥100 kHz are defined in terms of the *rms* value, while those at <100 kHz are defined in terms of the temporal peak value.

2.3 KDB Submission

In this section, we summarize situations where a KDB Inquiry is needed to demonstrate compliance of WPT devices. As stated in FCC KDB 680106 D01 [2]: *"WPT equipment manufacturers may have to use the KDB Inquiry process to provide documentation demonstrating how the device meets the requirements of this guidance, and only proceed with device authorization upon receiving concurrence from the FCC."*

The following are topics listed in FCC KDB 680106 D01 for submitting a KDB Inquiry:

- **Distance:** If the WPT device does not comply with RF exposure limits for some unlikely use conditions, a KDB Inquiry is needed (in accordance also with Section 3.3 of KDB 951290 D01 [7]). Information to be covered in the KDB Inquiry includes the selection of the minimum distance, an explanation for why this minimum distance was chosen, and reassurance that any non-compliant use conditions (e.g., getting closer than the minimum distance selected) are highly unlikely to occur.

- **Part 18 WPT devices:** For a WPT device whose charging function is intended for operation under 47 CFR Part 18 (industrial, scientific, and medical equipment), the KDB Inquiry process is required to obtain FCC concurrence, unless exception criteria in Section 5.2 (1) through (6) of KDB 680106 [2] are met. Information to be covered in the KDB Inquiry includes the operating frequency, the conducted power for each radiating structure, operation scenarios, RF exposure compliance information, and the maximum charging distance between the load and the WPT transmitter.

- **WPT "at a distance":** Part 18 WPT transmitters that can provide power to a load beyond a separation distance of 1 m require a KDB Inquiry, in accordance also with Section 3.2 of KDB 951290 D01 [7].

Note: FCC KDB 680106 [2] requires submission of a KDB Inquiry to the FCC for compliance testing of WPT devices in most cases. We recommend that the following statement be included in the inquiry: *"The evaluation is performed according to the attached Application Note "Testing WPT Devices with DASY8/6 Modules WPT and SAR for Compliance with FCC KDB 447498/680106" issued by SPEAG."*

3 SPEAG's Measurement Solutions

3.1 DASY8/6 Module SAR V16.2+

DASY8/6 Module SAR V16.2+ meets all performance requirements of IEC/IEEE 62209-1528:2020 [8] and FCC KDB 447498 [1] for frequencies between 4 MHz and 10 GHz. More details about DASY8/6 Module SAR 16.2+ are provided in the DASY8/6 Module SAR 16.2+ Manual [9].

3.2 DASY8/6 Module WPT V2.4+

DASY8/6 Module WPT V2.4+ meets all performance requirements of IEC/IEEE 63814 [10]. It is composed of the isotropic probe MAGPy-8H3D+E3D Version 2, the reference probe (MAGPy-RAϕV2), and the data acquisition system (MAGPy-DAS) mounted to the DASY8/6 robot via the emergency stop (MAGPy-ES). At each probe location, eight isotropic H-field values plus the phase are acquired in addition to the isotropic E-field measurement.

The field is measured on a high density grid (7.33 mm resolution) such that the incident quasi-static H-field (amplitude and phase) in the entire measured volume can be reconstructed by means of our advanced and validated vector potential reconstruction (see Appendix A for more information). The incident E-field distribution is measured in the same volume, enabling accurate determination of the field impedance at $d = 30$ mm. Due to the geometric design of the E_z-field sensor, the measured information is sufficient for a reliable estimation of the E-fields at the surface of the DUT, i.e., the distance $d = 0$, and its potential coupling to the tissue simulating media, even for very localized E-field sources. The energy absorbed in the phantom, compared to the energy stored in the H-field, is very small for frequencies <4 MHz (see Appendix B), i.e., < -20 dB (<1%). Therefore, the incident field is not affected by the presence of the phantom for inductive sources.

The measured and reconstructed fields are used to assess the SAR induced by the incident H-field, without approximation and with known uncertainty, by Sim4Life's Quasi-Static EM Solver (P-EM-QS) (ZMT Zurich MedTech AG). The SAR induced by the incident E-field[5] is determined by a conservative approximation that is valid for local E-field sources [11]. The validity of the local E-field condition is automatically assessed by the system, including a check on whether the field impedance is less than 10% of the plane wave impedance of 377 Ω.

The total field evaluation (see Appendix C for its validation) provides the assessed total peak spatial-average SAR values (psSAR1g/10g), which are compared to the SAR limits (≥100 kHz). At frequencies below 100 kHz, the maximum incident fields determined are compared to the MPE limits published by the FCC.

The dedicated graphical user interface (GUI) fully automates the testing workflow. More details about DASY8/6 Module WPT V2.4+ are provided below and in the DASY8/6 Module WPT V2.4+ Manual [6].

Note: The method implemented in DASY8/6 Module WPT V2.4+ is equivalent to determination of SAR by simulations conducted with the validated P-EM-QS solver of Sim4Life (see Appendix D) but without DUT modeling and the validation uncertainties. Thus, the method is much more accurate than compliance testing with simulations, since the only remaining uncertainty is the reconstruction and measurement uncertainty, which is typically less than 1.3 dB. For typical and realistic simulation modeling uncertainty, see [12].

---

[5] The strongest E-field generated by a WPT system is often traceable to local accumulation of charge, e.g., across a discrete capacitor (to achieve resonance) and at the end of conductors, that decays rapidly as a function of d at a rate of $1/d^4$ but can potentially induce fields in the body [11]. The problem that these charge accumulations are difficult to predict or accurately simulate is overcome with DASY8/6 Module WPT V2.4+, which determines the field characteristics with measurements.

4 Test System and Procedures for Frequencies ≥4 MHz

4.1 System Requirements

DASY8/6 Module SAR V16.2+ meets all performance requirements for measurements according to IEC/IEEE 62209-1528:2020 [8] and FCC KDB 447498 [1] for frequencies between 4 MHz and 10 GHz (see DASY8/6 Module SAR Manual [9]). To determine psSAR1g/10g as required by §1.1310 of the FCC rules [3], the following system configuration is recommended:

- DASY8/6 Module SAR software
- ELI phantom
- HBBL4-250Vx head simulating liquid
- EX3DVx probe with conversion factor assessment at 6 MHz (covers 4 MHz to 9 MHz) and 13 MHz (covers 9 MHz to 19 MHz)
- confined loop antennas CLA-6 and CLA-13 for system check and validation purposes

4.2 Measurement Procedure

The workflow to demonstrate compliance of WPT devices and systems operating at frequencies of >4 MHz with SAR limits is illustrated in Figure 1.3.

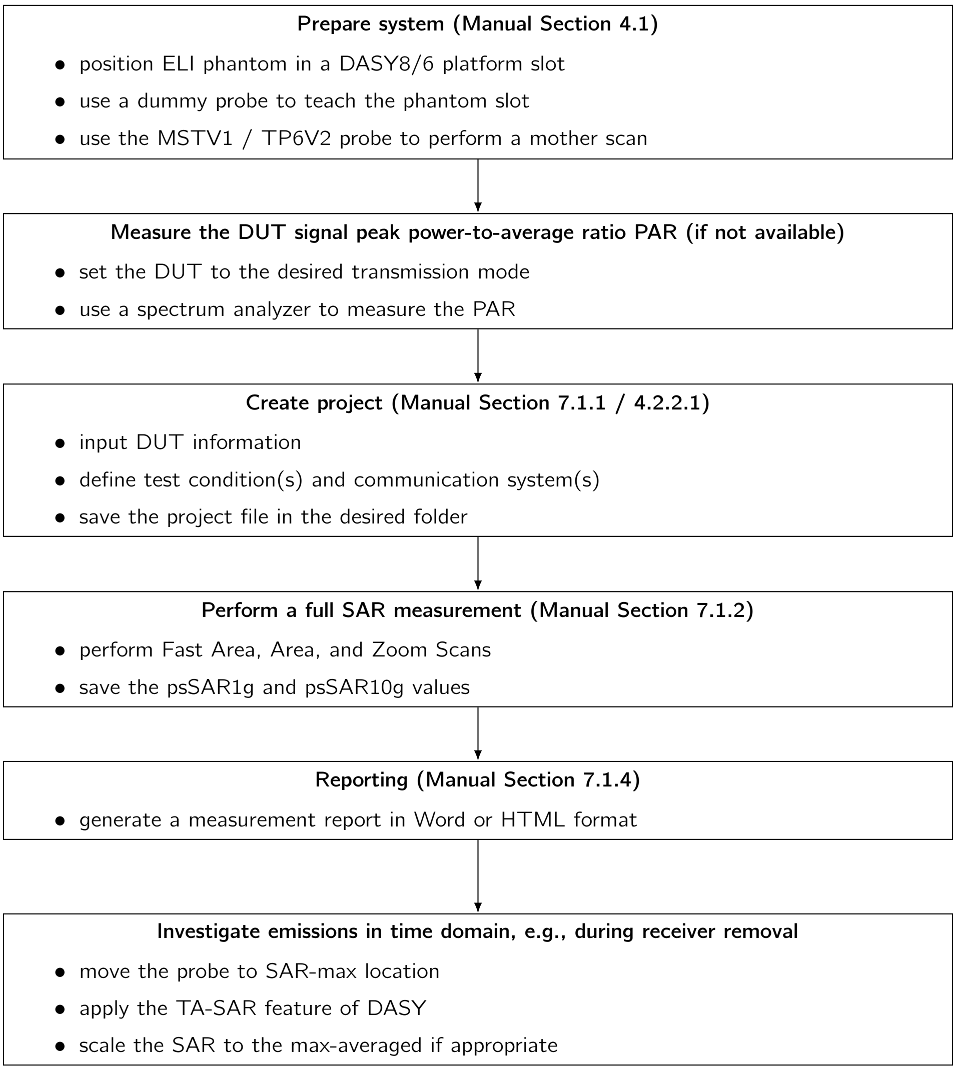

Prepare system (Manual Section 4.1)

- position ELI phantom in a DASY8/6 platform slot
- use a dummy probe to teach the phantom slot
- use the MSTV1 / TP6V2 probe to perform a mother scan

Measure the DUT signal peak power-to-average ratio PAR (if not available)

- set the DUT to the desired transmission mode
- use a spectrum analyzer to measure the PAR

Create project (Manual Section 7.1.1 / 4.2.2.1)

- input DUT information
- define test condition(s) and communication system(s)
- save the project file in the desired folder

Perform a full SAR measurement (Manual Section 7.1.2)

- perform Fast Area, Area, and Zoom Scans
- save the psSAR1g and psSAR10g values

Reporting (Manual Section 7.1.4)

- generate a measurement report in Word or HTML format

Investigate emissions in time domain, e.g., during receiver removal

- move the probe to SAR-max location
- apply the TA-SAR feature of DASY
- scale the SAR to the max-averaged if appropriate

Figure 1.3: Step-by-step measurement procedure for using DASY8/6 Module SAR to evaluate compliance of WPT devices and systems with SAR limits when operating at frequencies >4 MHz.

4.3 Uncertainty

The uncertainty for evaluations performed with DASY8/6 Module SAR 16.2+ was determined according to IEC/IEEE 62209-1528:2020 [8] and documented in the DASY8/6 Module SAR 16.2+ Manual [9]. Typically, the uncertainty ($k = 2$) is <22.8% for psSAR1g/10g (see Table 1.1).

DASY8/6 Uncertainty Budget
According to IEC/IEEE 62209-1528
(Frequency band: 4 MHz–300 MHz)

Symbol	Error Description	Unc. Value	Prob. Dist.	Div.	(c_i) (1 g)	(c_i) (10 g)	Std. Unc. (1 g)	Std. Unc. (10 g)
Measurement System Errors								
CF	Probe Calibration	±13.3%	N	2	1	1	±6.65%	±6.65%
CF_{drift}	Probe Calibration Drift	±1.7%	R	$\sqrt{3}$	1	1	±1.0%	±1.0%
LIN	Probe Linearity	±4.7%	R	$\sqrt{3}$	1	1	±2.7%	±2.7%
BBS	Broadband Signal	±0.6%	R	$\sqrt{3}$	1	1	±0.3%	±0.3%
ISO	Probe Isotropy	±7.6%	R	$\sqrt{3}$	1	1	±4.4%	±4.4%
DAE	Other Probe+Electronic	±0.8%	N	1	1	1	±0.8%	±0.8%
AMB	RF Ambient	±1.8%	N	1	1	1	±1.8%	±1.8%
Δ_{sys}	Probe Positioning	±0.006 mm	N	1	0.04	0.04	±0.10%	±0.10%
DAT	Data Processing	±1.2%	N	1	1	1	±1.2%	±1.2%
Phantom and Device Errors								
LIQ(σ)	Conductivity (meas.)	±2.5%	N	1	0.78	0.71	±2.0%	±1.8%
LIQ(T_σ)	Conductivity (temp.)	±5.4%	R	$\sqrt{3}$	0.78	0.71	±2.4%	±2.2%
EPS	Phantom Permittivity	±14.0%	R	$\sqrt{3}$	0	0	±0%	±0%
DIS	Distance DUT – TSL	±2.0%	N	1	2	2	±4.0%	±4.0%
D_{xyz}	Device Positioning	±1.0%	N	1	1	1	±1.0%	±1.0%
H	Device Holder	±3.6%	N	1	1	1	±3.6%	±3.6%
MOD	DUT Modulation	±2.4%	R	$\sqrt{3}$	1	1	±1.4%	±1.4%
TAS	Time-average SAR	±1.7%	R	$\sqrt{3}$	1	1	±1.0%	±1.0%
RF_{drift}	DUT drift	±2.5%	N	1	1	1	±2.5%	±2.5%
VAL	Val Antenna Unc.	±0.0%	N	1	1	1	±0%	±0%
RF_{in}	Unc. Input Power	±0.0%	N	1	1	1	±0%	±0%
Correction to the SAR results								
C(ε, σ)	Deviation to Target	±1.9%	N	1	1	0.84	±1.9%	±1.6%
C(R)	SAR scaling	±0.0%	R	$\sqrt{3}$	1	1	±0.0%	±0.0%
u(ΔSAR)	Combined Uncertainty						±11.4%	±11.3%
U	**Expanded Uncertainty**						±22.8%	±22.5%

Table 1.1: Uncertainty budget for peak 1 gram and 10 gram mass-average SAR measured with DASY8/6 Module SAR, assessed according to IEC/IEEE 62209-1528.

5 Test System and Procedures for Frequencies from 100 kHz to 4 MHz

5.1 System Requirements

To determine psSAR1g/10g as required by §1.1310 of the FCC rules [3] at frequencies <4 MHz (note that the SAR limit from FCC stops at 100 kHz, while the frequency range supported by Module WPT stops at 3 kHz), the following equipment is required:

- DASY8/6 Module WPT V2.4+ including:
  - MAGPy-8H3D+E3D Version 2 probe with the integrated data acquisition system MAGPy-DAS
  - MAGy-RAϕV2 reference probe as a phase reference
  - MAGPy-ES emergency stop system
- WPT source V-Coil50/400 for system check and validation purposes
- Software DASY6/8 Module WPT V2.4+

5.2 Assessment of psSAR1g/10g

The workflow to demonstrate compliance of WPT devices and systems with SAR limits when operating in the frequency range from 100 kHz to 4 MHz is illustrated in Figure 1.4. Detailed descriptions of each step can be found in Section 7 of the DASY8/6 Module WPT V2.4+ Manual [6].

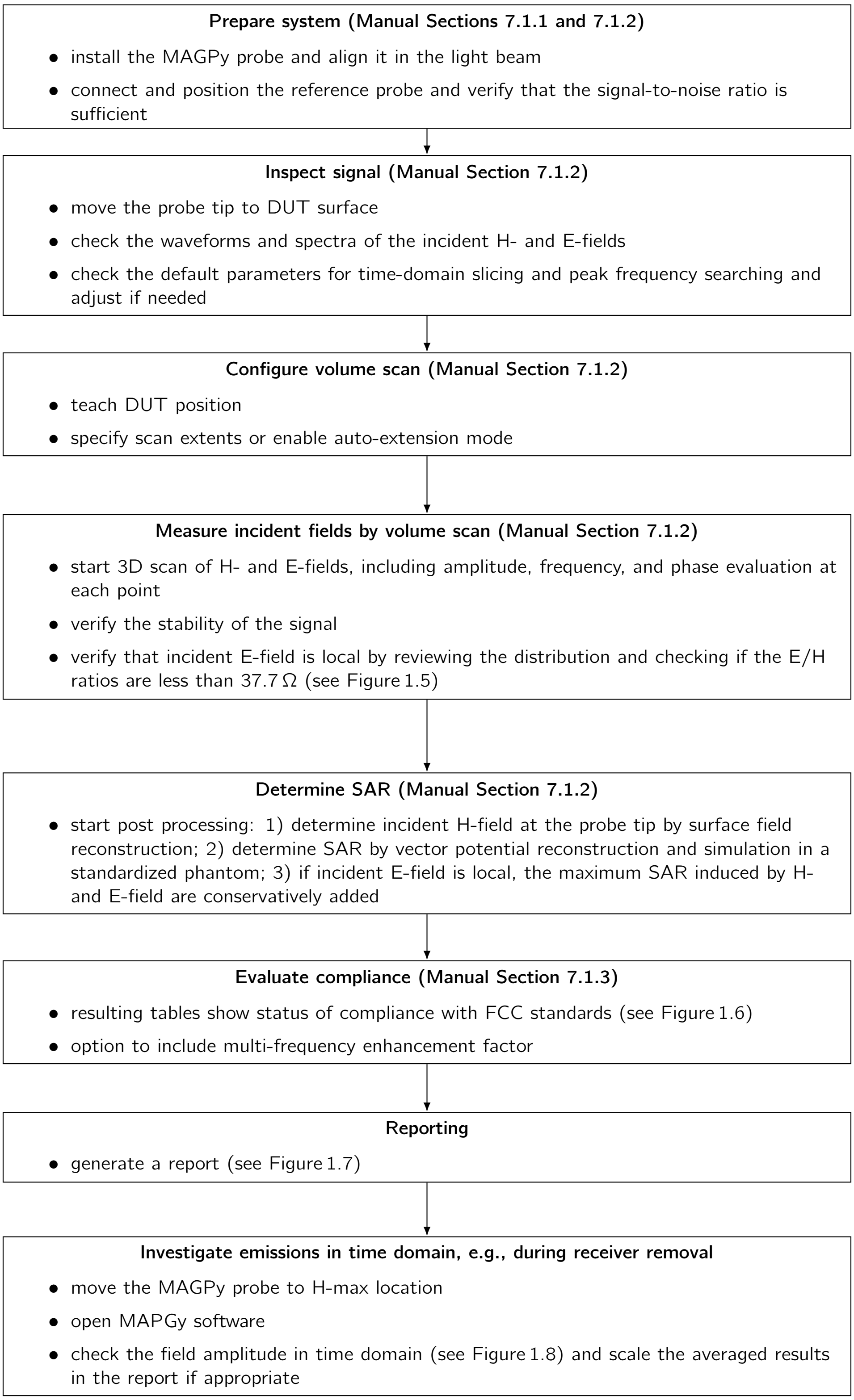

Prepare system (Manual Sections 7.1.1 and 7.1.2)

- install the MAGPy probe and align it in the light beam
- connect and position the reference probe and verify that the signal-to-noise ratio is sufficient

Inspect signal (Manual Section 7.1.2)

- move the probe tip to DUT surface
- check the waveforms and spectra of the incident H- and E-fields
- check the default parameters for time-domain slicing and peak frequency searching and adjust if needed

Configure volume scan (Manual Section 7.1.2)

- teach DUT position
- specify scan extents or enable auto-extension mode

Measure incident fields by volume scan (Manual Section 7.1.2)

- start 3D scan of H- and E-fields, including amplitude, frequency, and phase evaluation at each point
- verify the stability of the signal
- verify that incident E-field is local by reviewing the distribution and checking if the E/H ratios are less than 37.7 Ω (see Figure 1.5)

Determine SAR (Manual Section 7.1.2)

- start post processing: 1) determine incident H-field at the probe tip by surface field reconstruction; 2) determine SAR by vector potential reconstruction and simulation in a standardized phantom; 3) if incident E-field is local, the maximum SAR induced by H- and E-field are conservatively added

Evaluate compliance (Manual Section 7.1.3)

- resulting tables show status of compliance with FCC standards (see Figure 1.6)
- option to include multi-frequency enhancement factor

Reporting

- generate a report (see Figure 1.7)

Investigate emissions in time domain, e.g., during receiver removal

- move the MAGPy probe to H-max location
- open MAPGy software
- check the field amplitude in time domain (see Figure 1.8) and scale the averaged results in the report if appropriate

Figure 1.4: Step-by-step measurement procedure for using DASY8/6 Module WPT to evaluate compliance of WPT devices and systems with SAR limits when operating over the frequency range 100 kHz – 4 MHz.

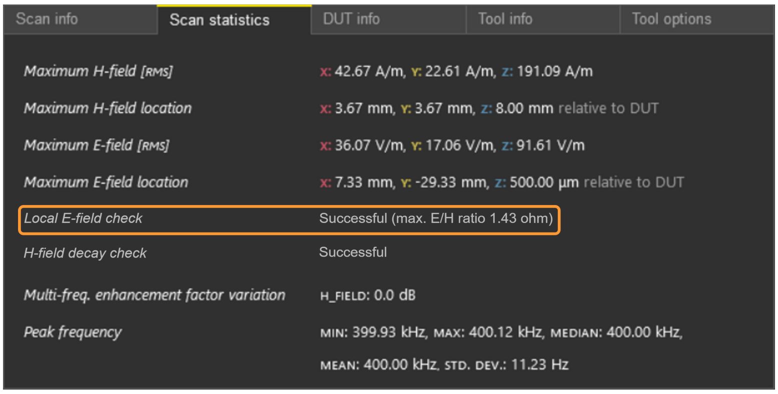

Maximum H-field [RMS] x: 42.67 A/m, y: 22.61 A/m, z: 191.09 A/m

Maximum H-field location x: 3.67 mm, y: 3.67 mm, z: 8.00 mm relative to DUT

Maximum E-field [RMS] x: 36.07 V/m, y: 17.06 V/m, z: 91.61 V/m

Maximum E-field location x: 7.33 mm, y: -29.33 mm, z: 500.00 µm relative to DUT

Local E-field check Successful (max. E/H ratio 1.43 ohm)

H-field decay check Successful

Multi-freq. enhancement factor variation H_FIELD: 0.0 dB

Peak frequency MIN: 399.93 kHz, MAX: 400.12 kHz, MEDIAN: 400.00 kHz, MEAN: 400.00 kHz, STD. DEV.: 11.23 Hz

Figure 1.5: The section of the DASY8/6 Module WPT GUI that displays the statistical information of the volume scan, e.g., the result of the local E-field check (highlighted by the orange box; the maximum E/H ratio is also listed).

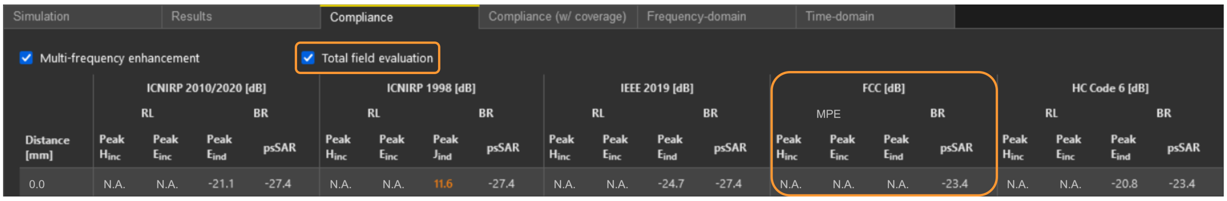

☑ Multi-frequency enhancement ☑ Total field evaluation

	ICNIRP 2010/2020 [dB]				ICNIRP 1998 [dB]				IEEE 2019 [dB]				FCC [dB]				HC Code 6 [dB]			
	RL		BR		RL		BR		RL		BR		MPE		BR		RL		BR	
Distance [mm]	Peak H_{inc}	Peak E_{inc}	Peak E_{ind}	psSAR	Peak H_{inc}	Peak E_{inc}	Peak J_{ind}	psSAR	Peak H_{inc}	Peak E_{inc}	Peak E_{ind}	psSAR	Peak H_{inc}	Peak E_{inc}	Peak E_{ind}	psSAR	Peak H_{inc}	Peak E_{inc}	Peak E_{ind}	psSAR
0.0	N.A.	N.A.	-21.1	-27.4	N.A.	N.A.	11.6	-27.4	N.A.	N.A.	-24.7	-27.4	N.A.	N.A.	N.A.	-23.4	N.A.	N.A.	-20.8	-23.4

Figure 1.6: Table in the DASY8/6 Module WPT GUI showing the compliance evaluation results for the total induced SAR (i.e., for exposures from both incident H- and E-fields; note that the "Total field evaluation" option (highlighted by the orange box) is checked here).

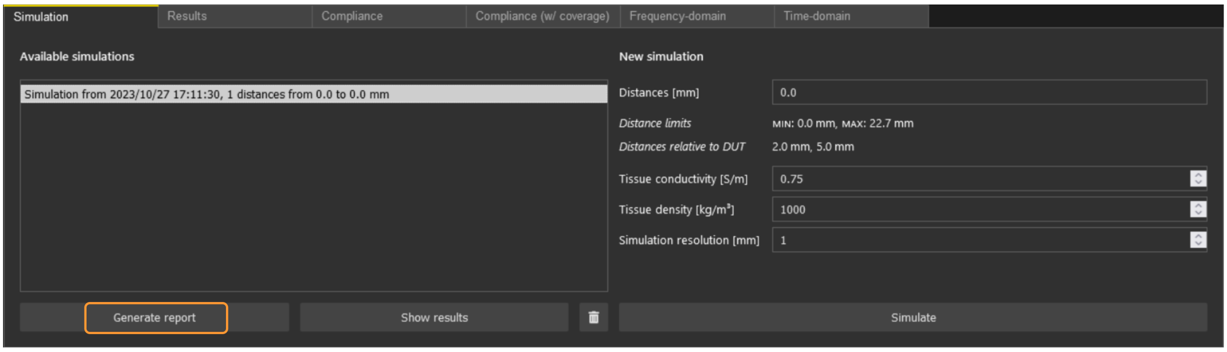

Available simulations

Simulation from 2023/10/27 17:11:30, 1 distances from 0.0 to 0.0 mm

New simulation

Distances [mm] 0.0
Distance limits MIN: 0.0 mm, MAX: 22.7 mm
Distances relative to DUT 2.0 mm, 5.0 mm
Tissue conductivity [S/m] 0.75
Tissue density [kg/m³] 1000
Simulation resolution [mm] 1

Figure 1.7: The section of the DASY8/6 Module WPT GUI for setting up the simulation and generating the report. After the simulation is completed, a report can be generated by clicking the "Generate report" button (highlighted by the orange box).

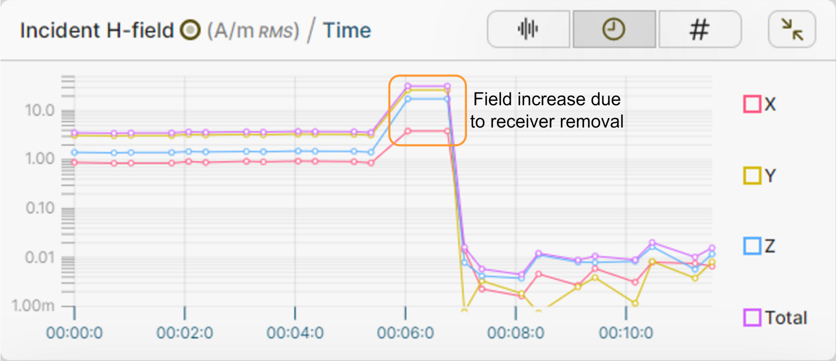

Figure 1.8: The time-domain plot of the incident H-field in the MAGPy graphical user interface. The data were recorded from a commercial wireless charger while removing the smartphone placed on the charger. The same procedure can also be used to monitor the stability of the source.

5.3 Uncertainty

The uncertainty for evaluations performed with DASY8/6 Module WPT V2.4+ was determined according to IEC/IEEE 63184 [10] and documented in the DASY8/6 Module WPT V2.4+ Manual [6]. Typically, the uncertainty ($k = 2$) is <33.9% for psSAR1g/10g (see Tables 1.2 and 1.3).

DASY8/6 Uncertainty Budget for psSAR1g
according to IEC/IEEE 63184

Item	Error Description	Unc. Value (±dB)	Probab. Distr.	Div.	(c_i)	Std. Unc. (±dB)
Measurement system						
1	Amplitude calibration uncertainty	0.35	N	1	1	0.35
2	Probe anisotropy	0.60	R	$\sqrt{3}$	1	0.35
3	Probe dynamic linearity	0.20	R	$\sqrt{3}$	1	0.12
4	Probe frequency domain response	0.30	R	$\sqrt{3}$	1	0.17
5	Probe frequency linear interp. fit	0.15	R	$\sqrt{3}$	1	0.09
6	Spatial averaging	0.10	R	$\sqrt{3}$	1	0.06
7	Parasitic E-field sensitivity	0.10	R	$\sqrt{3}$	1	0.06
8	Detection limit	0.15	R	$\sqrt{3}$	1	0.09
9	Readout electronics	0	N	1	1	0
10	Probe positioning	0.19	N	1	1	0.19
11	Repeatability	0.10	N	1	1	0.10
12	Surface field reconstruction	0.20	N	1	1	0.20
Numerical simulations						
13	Grid resolution	0.02	R	$\sqrt{3}$	1	0.01
14	Tissue parameters	0	R	$\sqrt{3}$	1	0
15	Exposure position	0	R	$\sqrt{3}$	1	0
16	Source representation	0.09	N	1	1	0.09
17	Convergence and power budget	0	R	$\sqrt{3}$	1	0
18	Boundary conditions	0.10	R	$\sqrt{3}$	1	0.06
19	Phantom loading/backscattering	0.10	R	$\sqrt{3}$	1	0.06
Combined uncertainty ($k = 1$)						0.63
Expanded uncertainty ($k = 2$)						**1.27 (33.9%)**

Table 1.2: Uncertainty budget for peak 1 gram mass-average SAR measured with DASY8/6 Module WPT, assessed according to IEC/IEEE 63184.

DASY8/6 Uncertainty Budget for psSAR10g

according to IEC/IEEE 63184

Item	Error Description	Unc. Value (±dB)	Probab. Distr.	Div.	(c_i)	Std. Unc. (±dB)
Measurement system						
1	Amplitude calibration uncertainty	0.35	N	1	1	0.35
2	Probe anisotropy	0.60	R	$\sqrt{3}$	1	0.35
3	Probe dynamic linearity	0.20	R	$\sqrt{3}$	1	0.12
4	Probe frequency domain response	0.30	R	$\sqrt{3}$	1	0.17
5	Probe frequency linear interp. fit	0.15	R	$\sqrt{3}$	1	0.09
6	Spatial averaging	0.10	R	$\sqrt{3}$	1	0.06
7	Parasitic E-field sensitivity	0.10	R	$\sqrt{3}$	1	0.06
8	Detection limit	0.15	R	$\sqrt{3}$	1	0.09
9	Readout electronics	0	N	1	1	0
10	Probe positioning	0.19	N	1	1	0.19
11	Repeatability	0.10	N	1	1	0.10
12	Surface field reconstruction	0.20	N	1	1	0.20
Numerical simulations						
13	Grid resolution	0	R	$\sqrt{3}$	1	0
14	Tissue parameters	0	R	$\sqrt{3}$	1	0
15	Exposure position	0	R	$\sqrt{3}$	1	0
16	Source representation	0.04	N	1	1	0.04
17	Convergence and power budget	0	R	$\sqrt{3}$	1	0
18	Boundary conditions	0.10	R	$\sqrt{3}$	1	0.06
19	Phantom loading/backscattering	0.10	R	$\sqrt{3}$	1	0.06
Combined uncertainty ($k = 1$)						0.63
Expanded uncertainty ($k = 2$)						**1.25 (33.4%)**

Table 1.3: Uncertainty budget for peak 10 gram mass-average SAR measured with DASY8/6 Module WPT, assessed according to IEC/IEEE 63184.

6 Test System and Procedures for Devices Operating at Frequencies from 3 kHz to 100 kHz

6.1 System Requirements

To determine the peak incident fields for assessment of compliance with MPE as required by §1.1310 of the FCC rules [3] at frequencies <100 kHz, the following equipment is required:

- DASY8/6 Module WPT V2.4+ including:
    - MAGPy-8H3D+E3D Version 2 probe with the integrated data acquisition system MAGPy-DAS
    - MAGy-RAϕV2 reference probe as a phase reference
    - MAGPy-ES emergency stop system
- WPT sources V-Coil500/3 and V-Coil350/85 for system check and validation purposes

6.2 Assessment of Peak Incident Fields

The workflow to demonstrate compliance with MPE is illustrated in Figure 1.9. Detailed descriptions of each step can be found in Section 7 of the DASY8/6 Module WPT V2.4+ Manual [6].

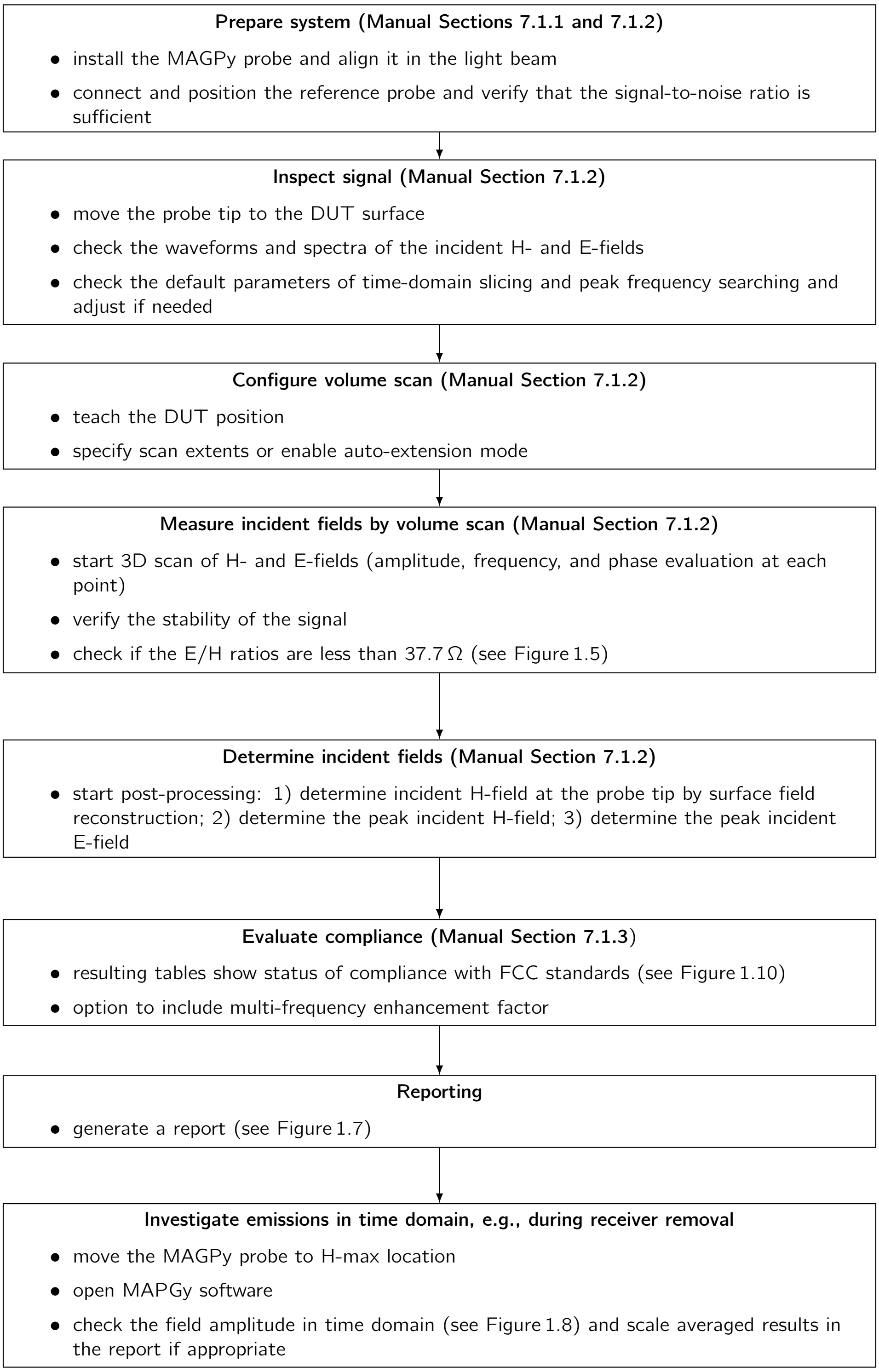

Prepare system (Manual Sections 7.1.1 and 7.1.2)

- install the MAGPy probe and align it in the light beam
- connect and position the reference probe and verify that the signal-to-noise ratio is sufficient

Inspect signal (Manual Section 7.1.2)

- move the probe tip to the DUT surface
- check the waveforms and spectra of the incident H- and E-fields
- check the default parameters of time-domain slicing and peak frequency searching and adjust if needed

Configure volume scan (Manual Section 7.1.2)

- teach the DUT position
- specify scan extents or enable auto-extension mode

Measure incident fields by volume scan (Manual Section 7.1.2)

- start 3D scan of H- and E-fields (amplitude, frequency, and phase evaluation at each point)
- verify the stability of the signal
- check if the E/H ratios are less than 37.7 Ω (see Figure 1.5)

Determine incident fields (Manual Section 7.1.2)

- start post-processing: 1) determine incident H-field at the probe tip by surface field reconstruction; 2) determine the peak incident H-field; 3) determine the peak incident E-field

Evaluate compliance (Manual Section 7.1.3)

- resulting tables show status of compliance with FCC standards (see Figure 1.10)
- option to include multi-frequency enhancement factor

Reporting

- generate a report (see Figure 1.7)

Investigate emissions in time domain, e.g., during receiver removal

- move the MAGPy probe to H-max location
- open MAPGy software
- check the field amplitude in time domain (see Figure 1.8) and scale averaged results in the report if appropriate

Figure 1.9: Step-by-step measurement procedure for using DASY8/6 Module WPT to evaluate compliance WPT devices and systems with MPE when operating at frequencies >100 kHz.

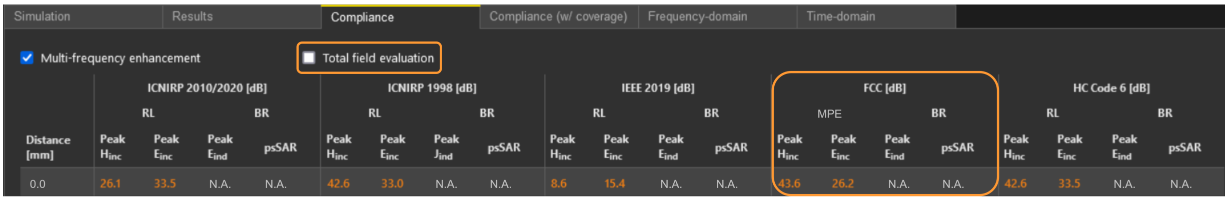

☑ Multi-frequency enhancement

☐ Total field evaluation

	ICNIRP 2010/2020 [dB]				ICNIRP 1998 [dB]				IEEE 2019 [dB]				FCC [dB]				HC Code 6 [dB]			
	RL		BR		RL		BR		RL		BR		MPE		BR		RL		BR	
Distance [mm]	Peak H_{inc}	Peak E_{inc}	Peak E_{ind}	psSAR	Peak H_{inc}	Peak E_{inc}	Peak J_{ind}	psSAR	Peak H_{inc}	Peak E_{inc}	Peak E_{ind}	psSAR	Peak H_{inc}	Peak E_{inc}	Peak E_{ind}	psSAR	Peak H_{inc}	Peak E_{inc}	Peak E_{ind}	psSAR
0.0	26.1	33.5	N.A.	N.A.	42.6	33.0	N.A.	N.A.	8.6	15.4	N.A.	N.A.	43.6	26.2	N.A.	N.A.	42.6	33.5	N.A.	N.A.

Figure 1.10: Table in the DASY8/6 Module WPT GUI showing the compliance evaluation results for the incident fields; note that the "Total field evaluation" option (highlighted by the orange box) is irrelevant here. Results for all induced field quantities are marked "N.A.", i.e., not applicable.

6.3 Uncertainty

The uncertainty for evaluations performed with DASY8/6 Module WPT V2.4+ was determined according to IEC/IEEE 63184 [10] and documented in the DASY8/6 Module WPT V2.4+ Manual [6]. Typically, the uncertainties ($k = 2$) are <16.6% for the incident H-field (at the lowest plane of the measurement volume, see Table 1.4) and <24.4% for the incident E-field (see Table 1.5).

DASY8/6 Uncertainty Budget for Peak Incident H-Field
according to IEC/IEEE 63184

Item	Error Description	Unc. Value (±dB)	Probab. Distr.	Div.	(c_i)	Std. Unc. (±dB)
Measurement system						
1	Amplitude calibration uncertainty	0.35	N	1	1	0.35
2	Probe anisotropy	0.60	R	$\sqrt{3}$	1	0.35
3	Probe dynamic linearity	0.20	R	$\sqrt{3}$	1	0.12
4	Probe frequency domain response	0.30	R	$\sqrt{3}$	1	0.17
5	Probe frequency linear interp. fit	0.15	R	$\sqrt{3}$	1	0.09
6	Spatial averaging	0.10	R	$\sqrt{3}$	1	0.06
7	Parasitic E-field sensitivity	0.10	R	$\sqrt{3}$	1	0.06
8	Detection limit	0.15	R	$\sqrt{3}$	1	0.09
9	Readout electronics	0	N	1	1	0
10	Probe positioning	0.19	N	1	1	0.19
11	Repeatability	0.10	N	1	1	0.10
12	Surface field reconstruction	0.30	N	1	1	0.30
Combined uncertainty ($k = 1$)						0.67
Expanded uncertainty ($k = 2$)						**1.33 (16.6%)**

Table 1.4: Uncertainty budget for peak incident H-field measured with DASY8/6 Module WPT, assessed according to IEC/IEEE 63184.

DASY8/6 Uncertainty Budget for Incident E-Field
according to IEC/IEEE 63184

Item	Error Description	Unc. Value (±dB)	Probab. Distr.	Div.	(c_i)	Std. Unc. (±dB)
Measurement system						
1	Amplitude calibration uncertainty	0.53	N	1	1	0.53
2	Probe anisotropy	0.80	R	$\sqrt{3}$	1	0.46
3	Probe dynamic linearity	1.00	R	$\sqrt{3}$	1	0.58
4	Probe frequency domain response	0.30	R	$\sqrt{3}$	1	0.17
5	Probe frequency linear interp. fit	0.15	R	$\sqrt{3}$	1	0.09
6	Parasitic H-field sensitivity	0.20	R	$\sqrt{3}$	1	0.12
7	Detection limit	0.15	R	$\sqrt{3}$	1	0.09
8	Readout electronics	0	N	1	1	0
9	Repeatability	0.10	N	1	1	0.10
Combined uncertainty ($k = 1$)						0.95
Expanded uncertainty ($k = 2$)						**1.89 (24.4%)**

Table 1.5: Uncertainty budget for incident E-field measured with DASY8/6 Module WPT with linear gradients across the probe, assessed according to IEC/IEEE 63184.

7 Conclusions

This application note provides guidance on how to use DASY8/6 Module SAR 16.2+ and DASY8/6 Module WPT V2.4+ for measurement-based assessments of compliance with SAR and MPE limits as required by FCC KDB 447498 D01 [1] and FCC KDB 680106 [2] for inductive WPT devices.

Note: The coverage factor is always one, as SAR assessed in the standardized homogeneous flat phantom is always conservative for anatomical tissue distributions [13].

Bibliography

[1] FCC KDB 447498 D01 v06, *RF exposure procedures and equipment authorization policies for mobile and portable devices*, October 2015.

[2] FCC KDB 680106 D01 v04, *Equipment authorization of wireless power transfer devices*, October 2023.

[3] United States Code of Federal Regulations (CFR), Title 47, Section 1.1310, *Radiofrequency radiation exposure limits*, `https://www.ecfr.gov/current/title-47/chapter-I/subchapter-A/part-1/subpart-I/section-1.1310` (Accessed: 12-Dec-2023).

[4] FCC KDB 447498 D01 DR05, *RF exposure procedures and equipment authorization policies for mobile and portable devices*, draft for review, August 2022, `https://apps.fcc.gov/oetcf/kdb/reports/ExpiredDocumentList.cfm` (Accessed: 12-Dec-2023).

[5] FCC-19-126, ET Docket No. 19-226, *Targeted changes to the Commission's rules regarding human exposure to radiofrequency electromagnetic fields*, December 2019, `https://docs.fcc.gov/public/attachments/FCC-19-126A1$_$Rcd.pdf`, (Accessed: 12-Dec-2023).

[6] SPEAG, *DASY8/6 Module WPT system handbook, incl. SW module WPT 2.4*, February 2024.

[7] FCC KDB 951290 D01 v01, *Equipment compliance review (ECR) inquiries*, August 2023.

[8] IEC/IEEE 62209-1528:2020, *Measurement procedure for the assessment of specific absorption rate of human exposure to radio frequency fields from hand-held and body-worn wireless communication devices - Part 1528: Human models, instrumentation and procedures (Frequency range of 4 MHz to 10 GHz)*, October 2020.

[9] SPEAG, *DASY8/6 Module SAR system handbook, incl. SW module SAR 16.2*, May 2023.

[10] IEC/IEEE 63184, *Assessment methods of the human exposure to electric and magnetic fields from wireless power transfer systems – Models, instrumentation, measurement and computational methods and procedures (Frequency range of 3 kHz to 30 MHz)*, CDV, August 2023.

[11] Christ, A., Fallahi, A., Neufeld, E., Balzano, Q., and Kuster, N., *Mechanism of capacitive coupling of proximal electromagnetic sources with biological bodies*, Bioelectromagnetics, vol. 43, no. 7, pp. 404–412, 2022.

[12] SPEAG Application Note, *Testing WPT devices by simulations: Guidance for best practice*, January 2024.

[13] Xi, J., Christ, A., and Kuster, N., *Coverage factors for efficient demonstration of compliance of low-frequency magnetic near-field exposures with basic restrictions*, Physics in Medicine & Biology, vol. 68, no. 3, 2023.

[14] Laakso, I., De Santis, V., Cruciani, S., Campi, T., and Feliziani, M., *Modeling of induced electric fields based on incompletely known magnetic fields*, Physics in Medicine & Biology, vol. 62, no. 16, 2017.

A Reconstruct a Vector Potential $\vec{A}$ From a Magnetic Field

The induced current simulation requires a vector potential instead of the H-field as input. The vector potential $\vec{A}$ has the property of $\texttt{curl}(\vec{A}) = \vec{B}$ and, in free space, of $\vec{B} = \mu_0 \vec{H}$.

This equation is non-trivial, given that any additional gradient field fulfills $\texttt{curl}(\vec{A} + \texttt{grad}(\phi)) = \vec{B}$. Luckily, an explicit formula that requires the use of $\texttt{div}(\vec{B}) \equiv 0$ on a rectilinear grid can be derived [14]. For the x-component (others are cyclic permutations), the formula reads:

$$A_x = -\int_0^y \left[\frac{1}{3} B_z(x,v,z) + \frac{1}{6} B_z(x,v,0)\right] \texttt{d}v + \int_0^z \left[\frac{1}{3} B_y(x,y,w) + \frac{1}{6} B_y(x,0,w)\right] \texttt{d}w \qquad (1)$$

where the subscripts x, y, and z denote the components along their corresponding axes, and v and w denote the integration variables. The axes origin, i.e., the point where the path integrals begin to integrate, can be arbitrarily chosen. Currently, the most dominant location of the $\vec{B}$ field is chosen as the origin to minimize numerical integration artefacts. Details are provided in [14].

B Effect of Backscattering on the Source

B.1 Objectives

In this section, we assess the effect of the phantom loading or backscattering on the incident field for frequencies below 4 MHz by comparing the dissipated energy in the phantom to the H-field energy. The uncertainty in the determination of the induced fields due to the incident field without the phantom is also determined.

B.2 Theory

Maxwell's equation in the frequency domain (with linear constitutive material models) reads (see Sim4Life manual for details):

$$\begin{aligned}
\nabla \times \vec{E} &= -j\omega \vec{B} = -j\omega\mu \vec{H} \\
\nabla \times \vec{H} &= -j\omega \vec{D} + \vec{J} = -j\omega\epsilon \vec{E} + \sigma \vec{E} + \vec{J_0} \\
\nabla \times \vec{D} &= \nabla \cdot \epsilon \vec{E} = \rho \\
\nabla \times \vec{B} &= \nabla \cdot \mu \vec{H} = 0
\end{aligned} \tag{2}$$

With a vector potential $\vec{A}$ defined as $\nabla \times \vec{A} = \vec{B} = \mu \vec{H}$ (in the Coulomb gauge, i.e., $\nabla \cdot \vec{A} = 0$), the E-field can be written as $\vec{E} = -j\omega \vec{A} - \nabla\phi$, where ϕ is an additional scalar potential. The complex permittivity $\tilde{\epsilon} := \epsilon + \frac{\sigma}{j\omega}$ and the divergence-freeness of the $\vec{A}$ allows the $\nabla \times \vec{H}$ equation to be rewritten as

$$\nabla \times \frac{1}{\mu} \nabla \times \vec{A} = \underbrace{\omega^2 \tilde{\epsilon} \vec{A} - j\omega\tilde{\epsilon}\nabla\phi}_{:=\omega\texttt{-terms}} + \vec{J_0} \tag{3}$$

The H-field $\vec{H}$ is the *static* H-field, i.e., it is not altered by the induced E-field, if

$$\nabla \times \frac{1}{\mu} \nabla \times \vec{A} = \vec{J_0}, \tag{4}$$

i.e., the two ω-terms are negligible. In the following, the order-of-magnitude scalings of those 2 ω-terms are investigated. The order of magnitude can be estimated by means of the in-order-of notation $\mathcal{O}(\cdot)$.

Frequency [kHz]	Coil diameter [mm]	$\omega^2\epsilon\mu L^2$ [dB]	$\omega\sigma\mu L^2$ [dB]
3	454.0	−147.0	−48.7
85	200.0	−103.1	−33.9
400	52.5	−99.5	−43.7
1000	52.5	−83.5	−35.7
2000	52.5	−71.5	−29.7
4000	52.5	−59.5	−23.7

Table 6: Results of the calculations of the two ω-terms (i.e., $\omega^2\epsilon\mu L^2$ and $\omega\sigma\mu L^2$) for tissue material properties $\epsilon_r = 55$, $\sigma = 0.75$ S/m and a coil diameter of 52 mm. The coil diameter was used as the characteristic length.

Since in a vacuum there are no free charges, i.e., ρ vanishes, the scalar and vector potential are related as $\nabla \times \epsilon\nabla\phi = -j\omega\nabla \cdot \epsilon\vec{A}$. Given a characteristic length scale L to estimate the spatial derivations, the following relationship is provided: $\mathcal{O}(\tilde{\epsilon}\phi/L^2) = \mathcal{O}(\omega\tilde{\epsilon}A/L)$, i.e, ϕ scales like $\phi = \mathcal{O}(\omega A L)$. Application of the same scaling strategy to two ω-terms in (3) yields $\mathcal{O}(\omega^2\tilde{\epsilon}A)$ in both cases. Therefore, it can be estimated

$$\frac{\texttt{both-}\omega\texttt{-terms}}{\nabla \times \frac{1}{\mu} \times A\texttt{-term}} = \mathcal{O}(\omega^2\tilde{\epsilon}\mu L^2), \tag{5}$$

i.e., written with permittivity and conductivity, the ω-terms can be neglected when

$$\begin{aligned}
\omega^2\epsilon\mu L^2 &\ll 1 \\
\omega\sigma\mu L^2 &\ll 1
\end{aligned} \tag{6}$$

Calculated values for the two ω-terms of the tissue material properties $\epsilon_r = 55$, $\sigma = 0.75\,\mathrm{S/m}$ and a reference coil diameter, where the coil diameter was used as the characteristic length, are provided in Table 6. At 4 MHz, both values are much smaller than -20 dB, i.e., the quasi-static conditions can still be considered as valid.

B.3 Simulation Evidence

As a next step, we simulate the extent of back-scattering or the loading by the phantom by comparing the energy absorbed in the phantom to the maximum stored energy in the H-field. This ratio is expressed as

$$Q^{-1} = \frac{\text{power absorpbed in the phantom}}{2\pi f(\text{maximum energy stored})} = \frac{\int_V (\rho\ \mathrm{SAR})dV}{2\pi f W_H} \tag{7}$$

In Eqn. (7), the magnetic energy stored W_H is calculated by integrating the product of the H-field strength and the magnetic flux density over a volume that is sufficiently large for convergence, and the absorbed power in the phantom is calculated by integrating the product of the mass density and SAR over the entire volume of the phantom.

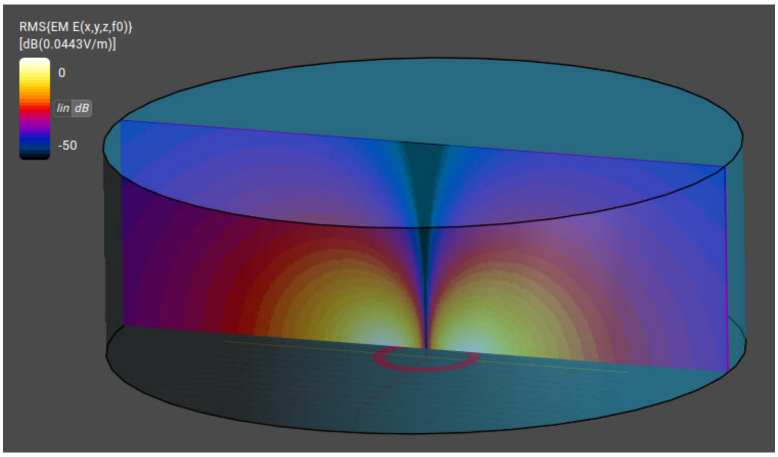

Figure 11: Normalized E-field of a generic WPT transmit coil with a diameter of 100 mm induced in a cylindrical phantom with a conductivity of 0.75 S/m placed at a distance of 4 mm.

Figure 11 shows an example of the E-field distribution in a cylindrical phantom positioned at a distance of 4 mm above a generic coil with a diameter of 100 mm simulated with the magneto quasistatic solver. According to the current draft of IEC 63184 [10], the relative permittivity of the tissue simulating liquid (TSL) in the phantom is $\epsilon_r = 55$, the conductivity $\sigma = 0.75\,\mathrm{S/m}$, and the density $\rho = 1000\,\mathrm{kg/m^3}$. The effect of the phantom on the total incident H-field along the vertical center line of the coil is shown in Figure 12. The Q^{-1} values according to Eqn. (7) for the generic coil at frequencies of 400 kHz and 6.78 MHz are given in Table 7.

Frequency [kHz]	W_H [μJ]	$\int_V(\rho\ \mathrm{SAR})dV$ [mW]	Q^{-1} [dB]
400	2.1	0.84	-30
6780	2.1	240	-18

Table 7: Maximum H-field energy and dissipated power in the phantom per $1\mathrm{A}_\mathrm{peak}$ for the 400 kHz and 6.78 kHz verification sources. The load of the phantom is <1% at frequencies <4 MHz.

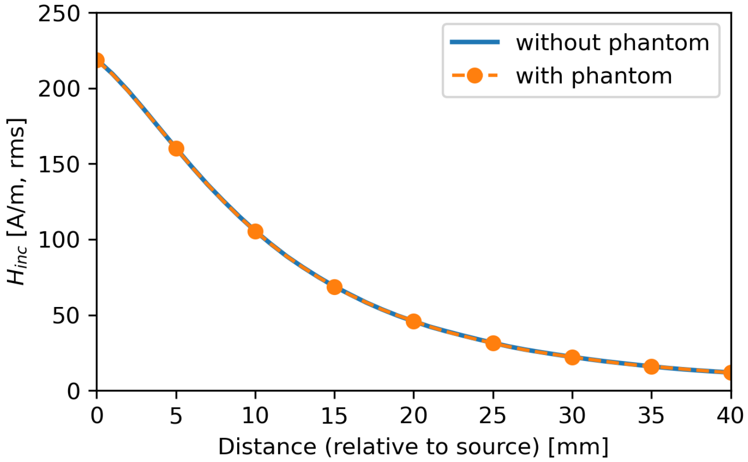

Figure 12: Comparison of the total incident H-fields (per $1\mathrm{A}_{\mathrm{peak}}$) along the *z*-axis center line of the coil with and without the phantom for the reference source V-Coil 50/400.

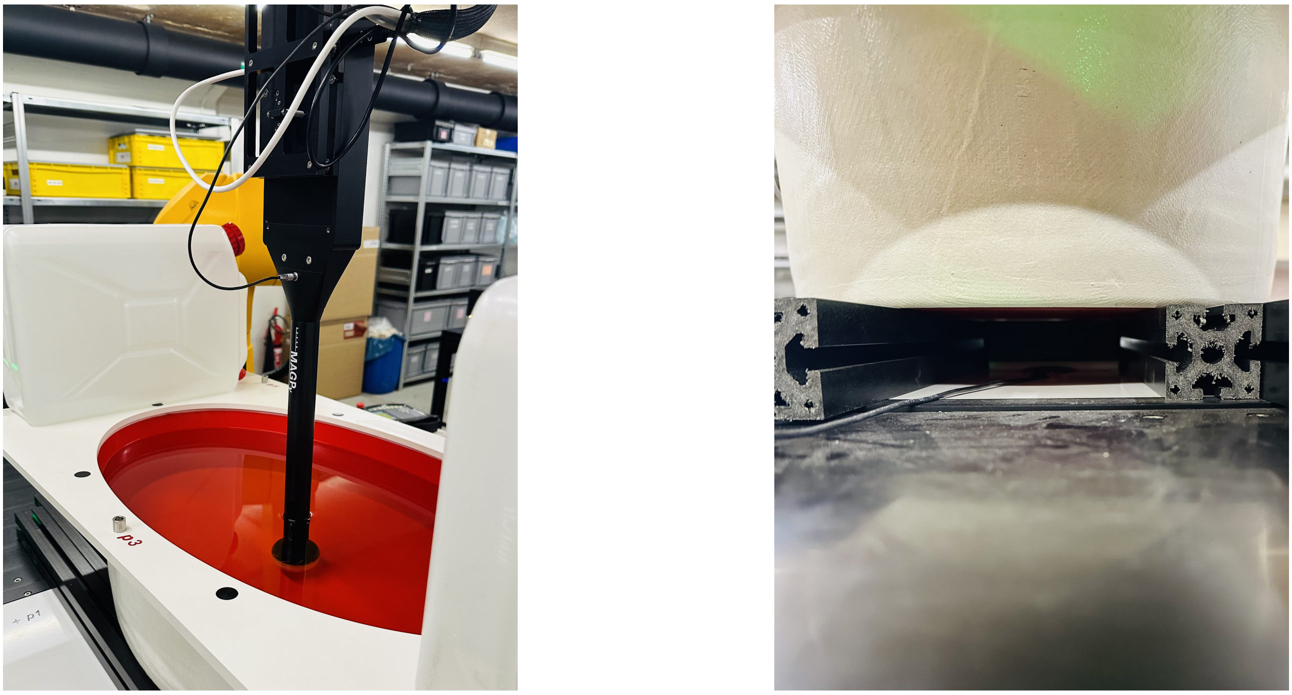

(a) Perspective view showing the probe measuring in TSL

(b) Side view showing the placement of the phantom and the source

Figure 13: Setup for experimental confirmation of incident H-field insensitivity to the presence of the phantom.

B.4 Experimental Confirmation

To experimentally confirm that the effect of the phantom on the incident H-field is very small, measurements were made with a specially sealed MAGPy probe placed inside the ELI phantom filled with tissue simulating liquid (TSL) HBBL4-250V3, which has the nominal values of $\epsilon_r = 55$ and $\sigma = 0.75\,\mathrm{S/m}$. The phantom was placed above the 400 kHz reference source (i.e., V-Coil50/400) at d $\approx$ 2 mm. The current fed to the coil was determined by measuring the voltage across the current monitoring resistor with an oscilloscope. A photo of the setup is shown in Figure 13. The probe was moved to different distances (with a DASY robot) along a vertical observation line. The incident H-field was measured at each distance for three cases: (1) without TSL, (2) with TSL of a filling depth of 105 mm, and (3) with TSL of a filling depth of 150 mm. The measurement for the case without TSL was repeated four times. The measurements for the cases with TSL were repeated twice, and were made between the second and third measurements for the case without TSL. The H-field measurement results are illustrated in Figure 14. The deviations are well within the expected measurement repeatability of $<$0.5 dB and confirms the theoretical considerations that the effect is less than 1% or 0.1 dB.

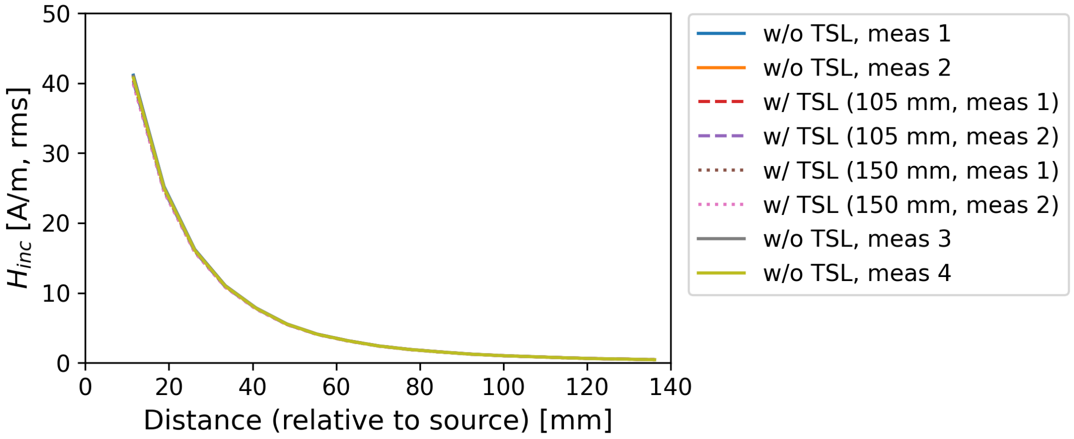

(a) Total H-fields along the vertical line for three TSL-filling cases

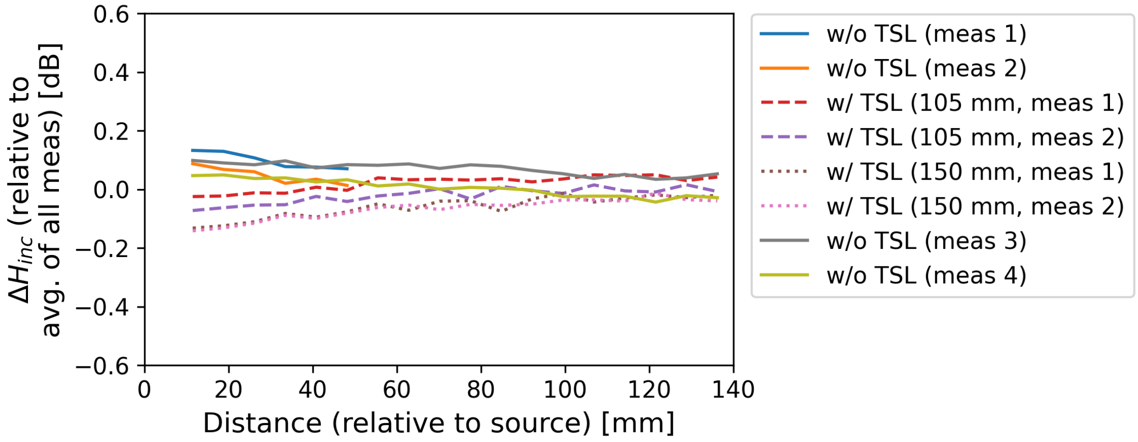

(b) Deviations in the total H-field along the vertical line for three TSL-filling cases

Figure 14: Measurement results of the incident H-field, confirming its insensitivity to the presence of the phantom. The results showed include three cases: with TSL of a filling depth of 105 mm, with TSL of a filling depth of 150 mm, without TSL.

B.5 Conclusions

The effect of the phantom loading or backscattering is less than 1% for frequencies <4 MHz as derived from theoretical considerations, supported by simulations and verified by measurements. Therefore, when the evaluation is performed on the incident field only, i.e., without phantom, the coupling between phantom and source results in an additional uncertainty of 0.1 dB.

C Validation of Total Field Evaluation of DASY8/6 Module WPT

C.1 Evaluation of the Induced Fields by the Validation Source V-Coil50/6780 V2

C.1.1 Instrumentation and V&V Sources

The configuration of the DASY8/6 Module WPT system used in the validation measurements is listed in Table 8.

System	Type:	DASY6 Module WPT
	Software Version:	V2.4
	Manufacturer:	Schmid & Partner Engineering AG, Switzerland
Positioner	Robot:	TX90 XL
	Serial No:	F/18/0004593/A/001
	Controller:	CS8C
	Serial No:	F/18/0004593/C/001
	Manufacturer:	Stäubli, France
Probe	Type:	MAGPy-8H3D+E3D V2
	Serial Number:	3065
	Calibrated On:	Apr. 6, 2023
	Next Calibration:	Apr. 2024
	Frequency Range:	3 kHz–10 MHz
	H-Field Dynamic Range:	0.1–3200 A/m
	E-Field Dynamic Range:	0.1–2000 V/m
	H-Field Sensor Area:	1 cm^2
	E-Field Sensor Length:	5 cm
	Probe Length:	335 mm
	Probe Tip Diameter:	60 mm (flat tip)
	Manufacturer:	Schmid & Partner Engineering AG, Switzerland
6.78 MHz Verification Source	Source Model:	V-Coil50/6780 V2
	Source Serial No.:	1014
	Source Dimensions:	250 mm × 125 mm × 35 mm
	Source Output Freq.:	6.78 MHz
	Source Current:	0.394 A
	Source Evaluated On:	Jan. 29, 2024
	Source Manufacturer:	Schmid & Partner Engineering AG, Switzerland

Table 8: DASY6 Module WPT system and Validation Source

C.1.2 Method

The 6.78 MHz validation source was simulated with the fullwave finite-difference time-domain solver and the magneto quasi-static (MQS) solver in Sim4Life V7.2, and also measured using DASY6 Module WPT V2.4. The total field approximation was also applied with the incident E-field obtained from simulation/measurement as the input. This is a nearly worst-case evaluation, as the contributions of the incident E-field to the induced E-field is further reduced at lower frequencies.

C.1.3 Results

The results are summarized in Table 9.

Simulation vs Measurement	Method	pE_{ind}[a] [V/m]	psSAR$_{1g}$ [W/kg]	psSAR$_{10g}$ [W/kg]
Simulation	Fullwave	109	4.05	1.97
	MQS	107	4.06	1.95
	Total field approximation	107	4.06	1.95
Measurement	MQS	104	3.97	1.97
	Total field approximation	104	3.97	1.97

[a] Maximum induced E-field

Table 9: Results of the induced field evaluations performed with Sim4Life V7.2 and DASY6 Module WPT V2.4.

C.2 Conclusions

The implemented MQS assessment provides accurate results for the fields induced by the incident H-field only. The total field approximation implemented in DASY8/6 Module WPT V2.4+ provides a reliable assessment of the maximum induced fields, e.g., psSAR1g/10g and pE_{ind}.

D Verification Report of Low Frequency Magneto Quasi-Static Solver

tHess
THESSALONIKI SOFTWARE SOLUTIONS

Verification Report MQS001AA201507

Sim4Life and SEMCAD X Low Frequency Magneto Quasi–Static Solver

George Tsanidis[1], Theodoros Samaras[2]

Thessaloniki, July 2015

[1]**THESS S.A., Technopolis ICT Business Park, 57001 Thessaloniki, Greece**
[2]**Department of Physics, Aristotle University of Thessaloniki, 54124 Thessaloniki, Greece**

Executive Summary

The THESS S.A. was mandated by ZMT Zurich MedTech AG (Offer No. 1420) to independently verify the Sim4Life and SEMCAD X platforms. The here documented MQS001AA201507 verification benchmark for the EM LF Magneto Quasi-static Solver was developed and tested for the Sim4Life Version v2.0 and SEMCAD X v14.8, and documented such that ZMT can automatically run the test for any new software version.

The MQS001AA201504 benchmark verifies the EM LF Magneto Quasi-static Solver against the analytically calculated value of the magnetic field generated by a circular thin-wire coil inside an adjacent conducting sphere. This benchmark tests the following solver features:

- that the EM LF Magneto Quasi-static Solver converges to the right solution
- that material interfaces are properly handled
- that the Biot-Savart sources are correctly implemented
- that post-processing correctly calculates derived quantities such as current density.

The agreement of the theoretically calculated magnetic field with the values derived from the Sim4Life and SEMCAD X platform is very good: The current density values at different positions inside the sphere match for the two methods with a deviation smaller than 0.5% for the finer discretization of the computational domain. With increasing grid resolution, the simulation results converge to the analytical solution.

In conclusion, the numerical MQS solver of Sim4Life and SEMCAD X therefore meets the requirements for modeling the magneto-quasistatic equation.

Contents

1 Objectives

The objective of this verification report MQS001AA201507 is to document the verification of the Sim4Life v2.0 and SEMCAD X v14.8 Low Frequency Magneto Quasi-static Solver by comparing numerical to analytical solutions of a specific problem.

The MQS solver first calculates a magneto-static vector potential (A_0) using the Biot-Savart law and subsequently determines the induced E-fields and currents using potential continuity while considering the inhomogeneous dielectric property distributions in the human anatomy [2]. The equation $\nabla \cdot \sigma \nabla \phi = -j\omega \nabla \cdot (\sigma A_0)$ is solved (σ: conductivity, ω: angular frequency, ϕ: electric scalar potential) which is valid at frequencies where ohmic currents dominate over displacement currents.

The following features of the EM LF Magneto Quasi-static solver have been identified as fundamental and requiring verification:

- that the EM LF Magneto Quasi-static Solver converges to the right solution
- that material interfaces are properly handled
- that the Biot-Savart sources are correctly implemented
- that post-processing correctly calculates derived quantities such as current density

For that purpose an analytically solvable benchmark case has been chosen such that it makes use and covers all of these critical features. The benchmark is a homogeneous sphere exposed to current carrying ring wire.

2 Methodology

2.1 Introduction

The field of Magnetostatics was widely studied during the 19th century. The work of J.B. Biot and F. Savart made possible the calculation of the magnetic field originating from an electric current. They provide an approximation of the Maxwell equations valid for low frequency, provided a quasi-static behavior that can be assumed in the case of slow time variations (low frequency) and sufficiently small dimensions. The approximation condition is $\left(\frac{d}{\lambda}\right)^2 << 1$, where d is the diameter of the computational domain and λ the wavelength. The law of Biot-Savart can be used in order to easily calculate the value of the magnetic field inside a head-sized sphere, with the dielectric properties of the human brain, created by an adjacent circular loop coil.

The numerically derived results of the EM LF Magneto Quasi-static Solver of the Sim4Life and SEMCAD X platform are compared with the theoretically calculated results in order to evaluate the reliability and accuracy of the former and this deviation is examined with respect to

- the relative solver tolerance used to terminate the numerical process,
- the grid step of the computational domain,
- the implementation of the material interfaces

2.2 Analytical solution

A surface coil (loop of uniform current) adjacent to a homogeneous conducting sphere can be used in order to predict the performance of MRI surface coils close to the human head. By solving the inhomogeneous boundary value problem of the system, the electromagnetic field inside the sphere can be calculated. The sphere's parameters, i.e. the relative dielectric constant ϵ_r and the conductivity σ, are chosen so as to model the human brain.

The magnetic field produced by the surface coil adjacent to the homogeneous sphere has been calculated by solving the inhomogeneous boundary value problem of a ring of radius R carrying uniform current I adjacent to a conducting dielectric sphere of radius α centered at the origin of a spherical coordinate system (Fig. 1).

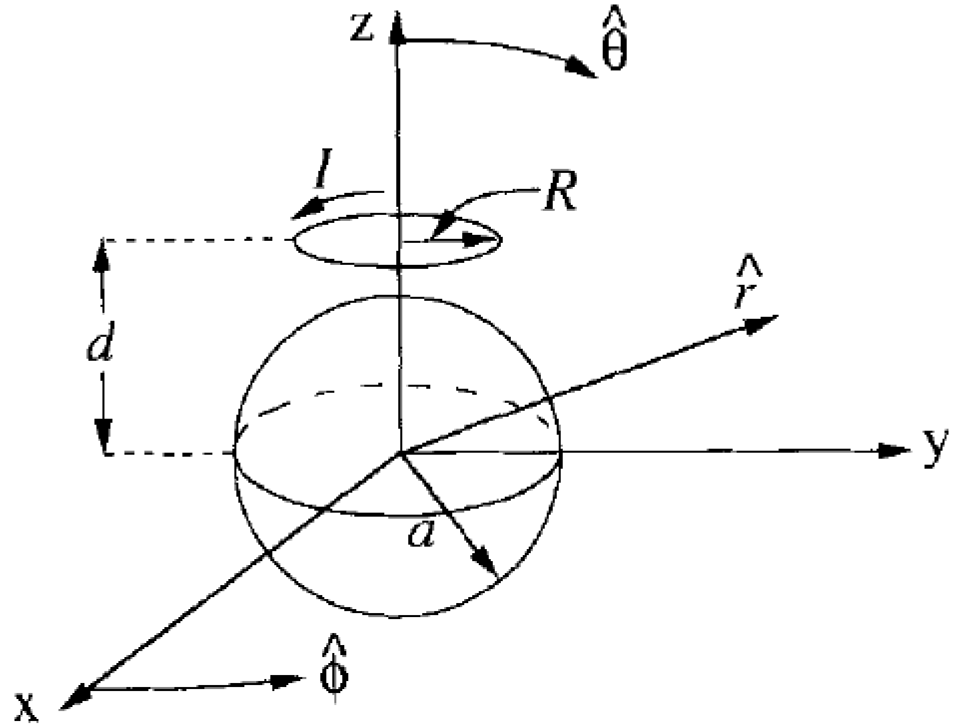

Figure 1: Schematic arrangement of a homogeneous conductive sphere near a circular current loop. The sphere is centered at the origin of the spherical coordinate system

The magnetic field inside the sphere is given by [1]

$$B_r(r,\theta,\phi) = \sum_{i=1}^{\infty} b_{l0}\sqrt{\frac{l(l+1)(2l+1)}{4\pi}}P_i(cos\theta)\frac{j_i(k^{in}r)}{k^{in}r} \tag{1}$$

$$B_\theta(r,\theta,\phi) = -\sum_{i=1}^{\infty} b_{l0}\sqrt{\frac{(2l+1)}{l(l+1)4\pi}}sin\theta\frac{dP_i(cos\theta)}{dcos\theta}\frac{1}{k^{in}r}\frac{\vartheta(j_i(k^{in}r))}{\vartheta r} \tag{2}$$

$$B_\phi(r,\theta,\phi) = 0 \tag{3}$$

where $j_i(kr)$ denotes the spherical Bessel functions of the first kind and $P_i(cos\theta)$ are Legendre polynomials.

The wavenumber inside the sphere k^{in} is obtained from Maxwell's equation ,

$$\nabla \times \vec{B} = \mu_0\vec{J} + \mu_0\epsilon\frac{\partial\vec{E}}{\partial t}. \tag{4}$$

where μ_0 is the permeability of free space. Substituting $\vec{J} = \sigma\vec{E}$ and defining the relative dielectric constant as $\epsilon_r = \frac{\epsilon}{\epsilon_0}$ equation (4) is transformed to

$$i\omega\nabla \times \vec{B} = (i\omega\mu_0\sigma + \epsilon_r\frac{\omega^2}{c^2})\vec{E} \tag{5}$$

where ω is angular frequency, σ is electrical conductivity and c is the speed of light. The wave number inside the sphere k^{in} is the square root of the coefficient of

$$(k^{in})^2 = i\omega\mu_0\sigma + \epsilon_r\frac{\omega^2}{c^2} \tag{6}$$

Solving equation (5) for the electric field, one is allowed to express the current density $\vec{J}$ as

$$J_{\phi}(r,\theta,\phi) = \frac{i\omega\sigma}{k^{in}} \sum_{i=1}^{\infty} b_{l0} \sqrt{\frac{(2l+1)}{l(l+1)4\pi}} j_i(k^{in}r) sin\theta \frac{dP_i(cos\theta)}{dcos\theta} \tag{7}$$

The b_{l0} are found by satisfying the boundary conditions of the magnetic field at the surface of a homogeneous conducting, dielectric sphere given an incident magnetic field produced by an adjacent ring of uniform current

$$\begin{aligned} b_{l0} = \mu_0 I 2\pi \sqrt{\frac{(2l+1)}{l(l+1)4\pi}} \frac{(k^{out})^2 R^2 {h_i}^{(1)}(k^{out}\sqrt{d^2+R^2})}{\sqrt{d^2+b^2}} \frac{dP_i(\xi)}{d\xi} \\ \frac{k^{in}(j_i(k^{out}\alpha)y_{i+1}(k^{out}\alpha) - y_i(k^{out}\alpha)j_{i+1}(k^{out}\alpha))}{k^{in}{h_i}^{(1)}(k^{out}\alpha)j_{i+1}(k^{in}\alpha) - k^{out}j_i(k^{in}\alpha){h_{i+1}}^{(1)}(k^{out}\alpha)} \end{aligned} \tag{8}$$

where k^{out} is the wave number in free space, y_i and ${h_i}^{(1)}$ are spherical Bessel functions of the second and third kinds, respectively, and ξ is the cosine of the angle subtended by the loop $\xi = \frac{d}{\sqrt{d^2+R^2}}$

2.3 Numerical Modeling

This verification study intends to compare the current density J calculated by the analytical solution, with the numerical results obtained by Sim4Life and SEMCAD X for the same problem. A sphere of 60mm radius and a surface coil of 20mm radius were placed at a distance of 50mm between the coil center and the nearest point of the sphere. For mathematical convenience the z axis of the coordinate system was chosen to be parallel to the axis of the coil. The sphere's relative dielectric permittivity ϵ_r and electrical conductivity σ are that of a human brain (white matter: $\sigma = 0.0626\, S/m$, $\epsilon_r = 69800$).

3 Results

3.1 Criterion of convergence

No difference in the numerical results was observed when changing the value of relative tolerance (which is the criterion of convergence for the computational process) from 10^{-6} to 10^{-12}. In particular the maximum difference between the values of the electric field induced inside the sphere, as extracted at the center, is 0.000172%.

3.2 Grid step

Simulations with uniform grids and varying grid step were performed (0.3, 0.5, 1, 2, 3, 4 and 5 mm) and they gave similar results (Fig. 2). For comparison the magnetic field along two axes (Fig. 3) was extracted and is presented with the theoretical, as is calculated by the Law of Biot-Savart (Fig. 4) and (Fig. 5).

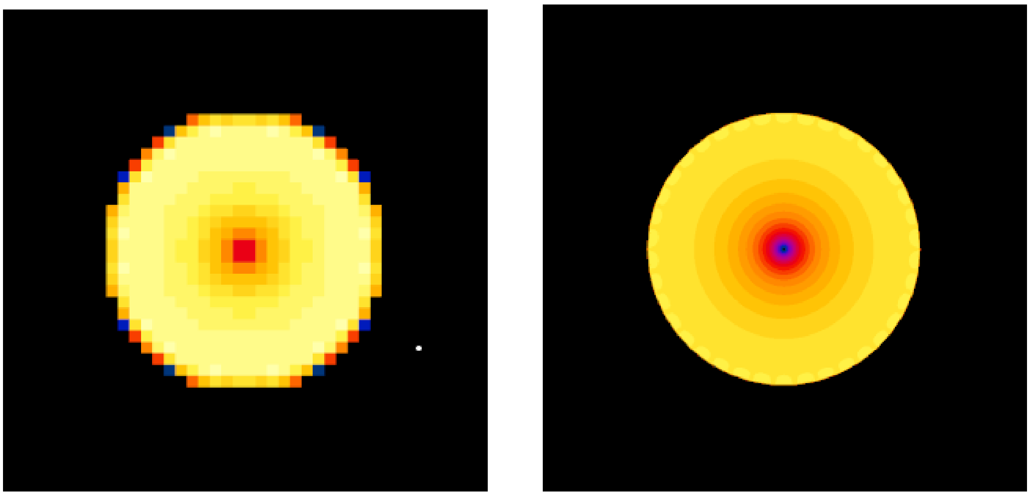

Figure 2: Slice views of the electric field inside the sphere for coarse (Grid Step: 5mm) and fine grid (Grid Step: 0.3mm).

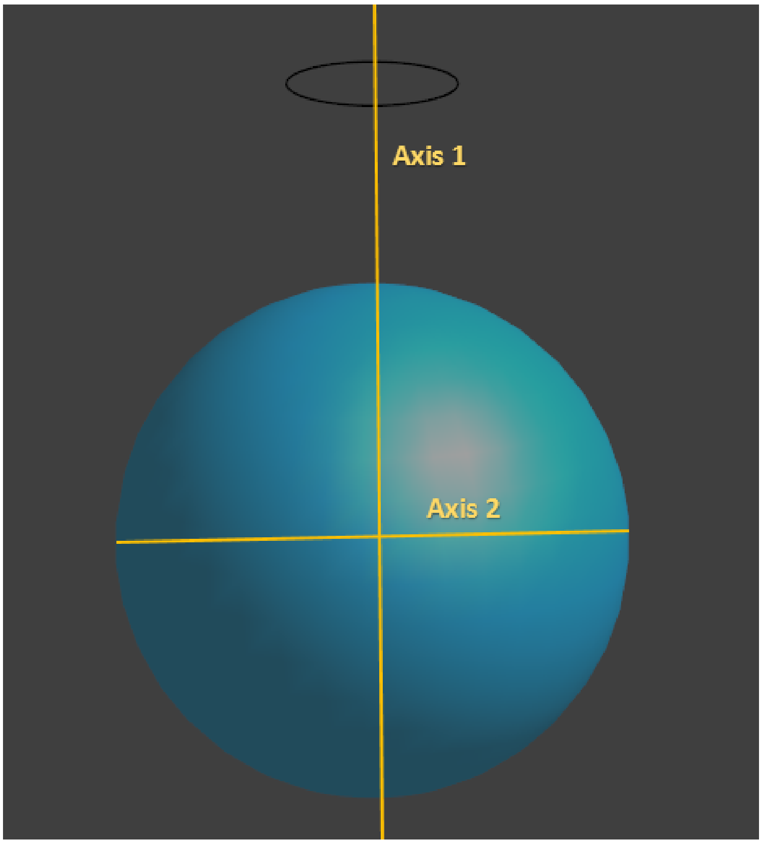

Figure 3: The two axes of extraction.

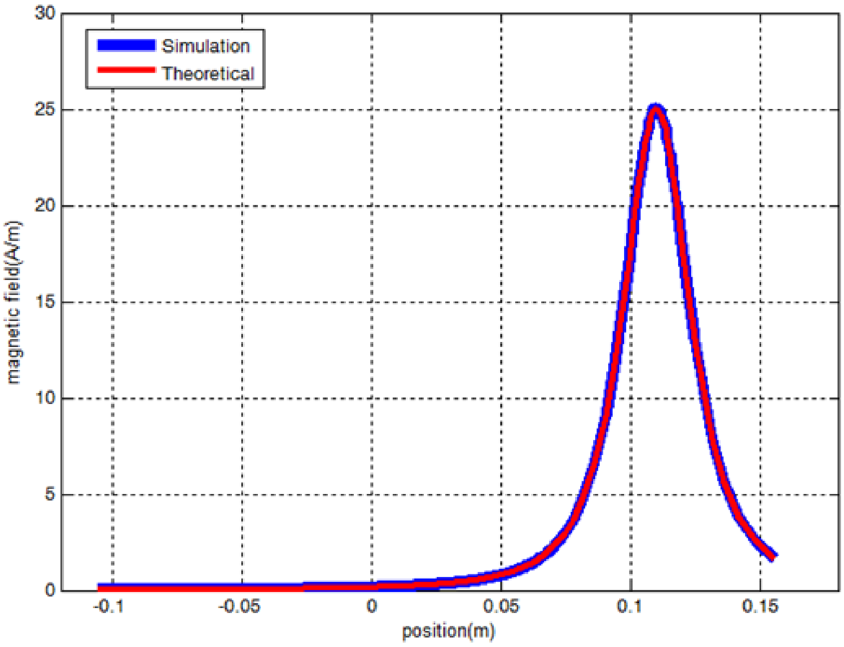

Figure 4: The extracted and the theoretical magnetic field along Axis 1 (Grid step: 0.3mm)

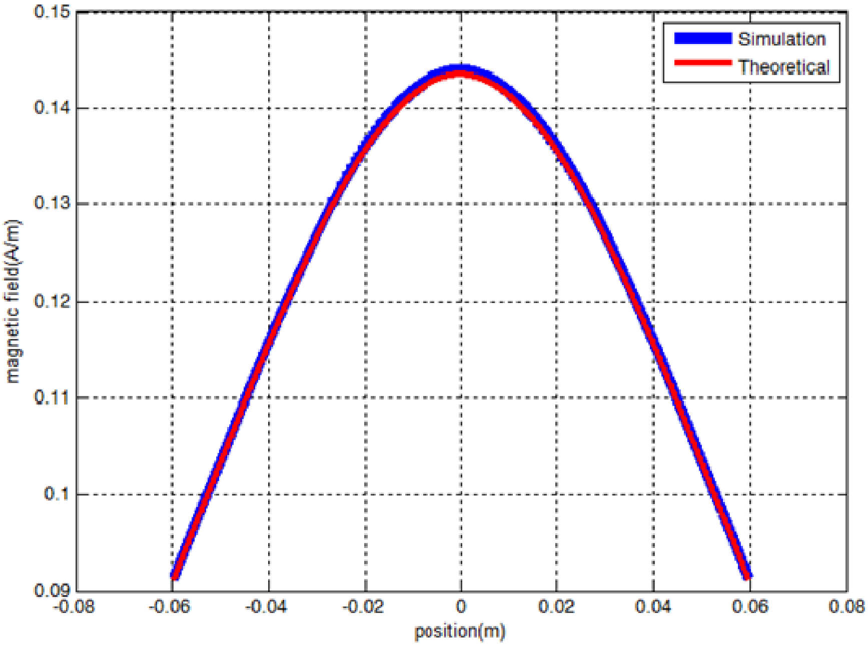

Figure 5: The extracted and the theoretical magnetic field along Axis 2 (Grid step: 0.3mm)

For the comparison between the theoretical and the simulated current distribution at the sphere, the deviation of the numerical solution from the analytical solution was evaluated at circles of distances 5, 10, 30 and 50mm from the center of the sphere(Fig. 6).

]
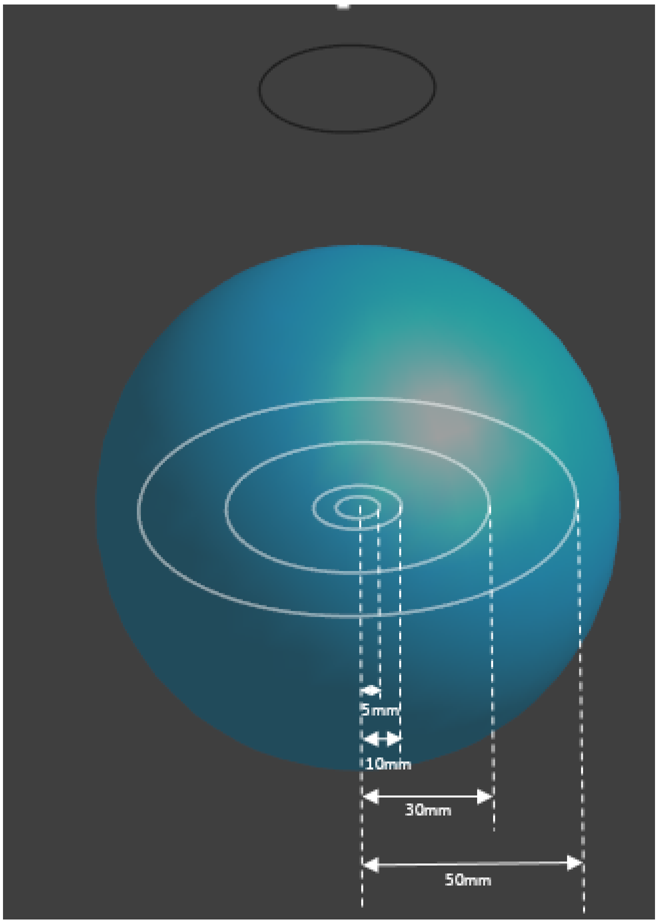

Figure 6: The two axes of extraction.

The computational space was discretized with a uniform grid of variable maximum step and the deviation between the numerical (N) and the analytical (T) solution for the current density was evaluated at the points of the numerical solution:

$$deviation\, U = |\frac{N-T}{T}|100\% \tag{9}$$

The maximum deviation on the above circles are shown in (Fig. 7). It is clear that, in every case, for a finer discretization of the grid (smaller grid step) the deviation continuously decreases and the numerical solution converges to the analytical solution.

3.3 Material interfaces

For the model with uniform grid step of 0.1mm, the radial component of the magnetic field was extracted on either side of the surface of the sphere, along a circle. At material interfaces, i.e., at the interface of air with the sphere, the radial component of the magnetic field should be identical when approaching the interface from both sides. The absolute value of the relative difference between the two values is shown in (Fig. 8). The deviation never exceeds 0.14% indicating that material interfaces are correctly handled by the solver.

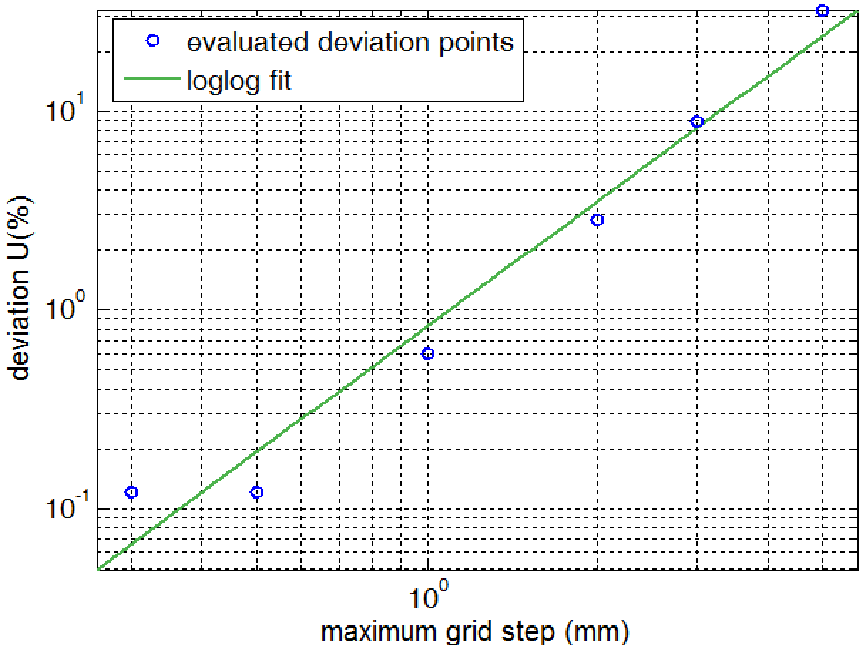
evaluated deviation points
loglog fit
10^1
10^0
10^{-1}
deviation U(%)
10^0
maximum grid step (mm)

]

(a)

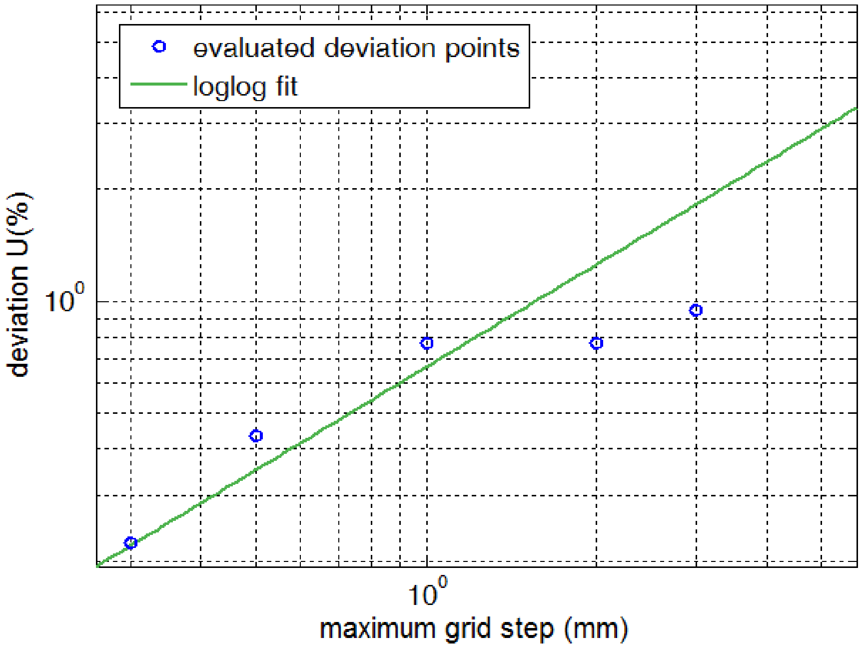
evaluated deviation points
loglog fit
10^0
deviation U(%)
10^0
maximum grid step (mm)

(b)

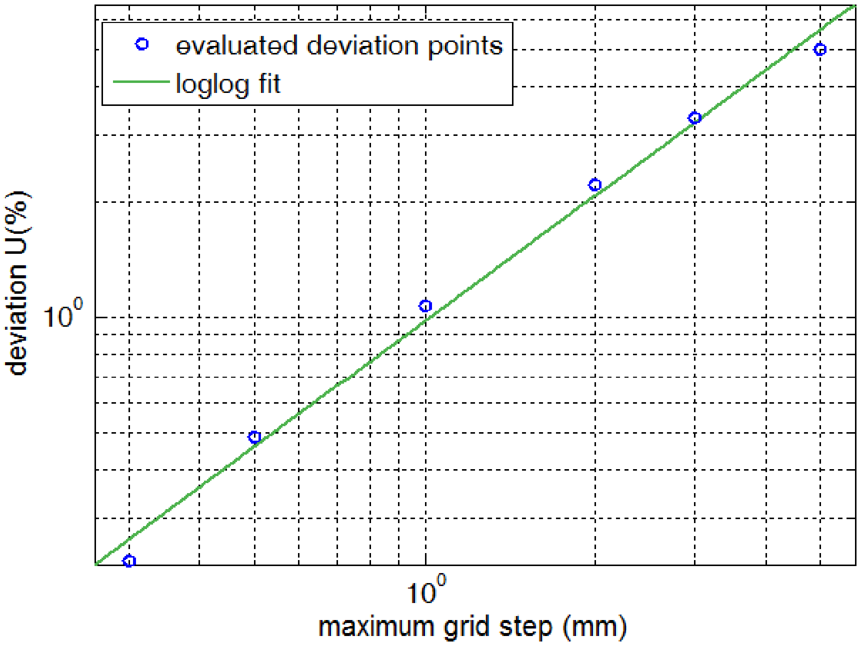

]

(a)

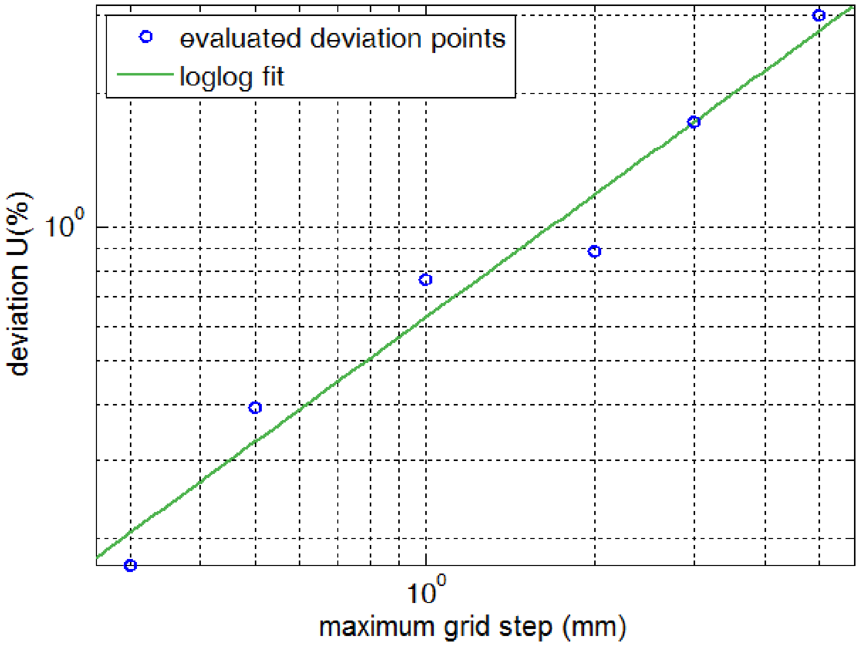

(b)

Figure 7: Maximum deviation (see equation (9)) of the numerical from the analytical solution along a circle at distance of 5mm (a), 10mm (b) 30mm (c) and 50mm (d) from the center of the sphere as a function of the maximum grid step.

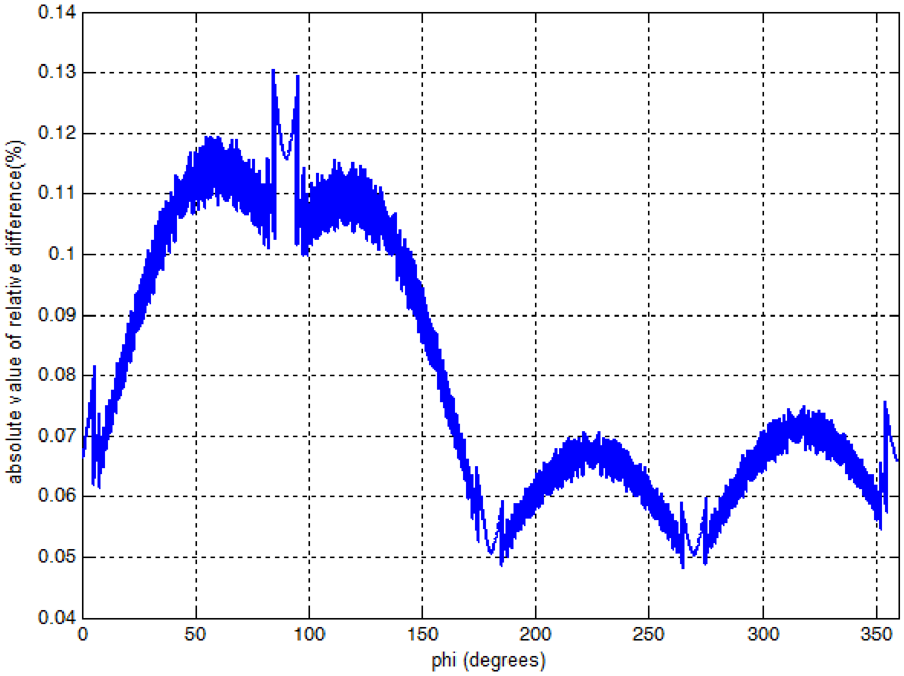

]

Figure 8: Relative difference (absolute value) between the perpendicular magnetic field components on either side of the sphere's surface. (Grid step: 0.1mm).

4 Conclusion

The purpose of this verification study was to examine the agreement between the numerical results obtained by the Sim4Life and SEMCAD X LF MagnetoQuasi-static solver and the analytically obtained results. It was shown that grid resolution has an important impact on accuracy. It is possible to keep the deviation between numerical and analytical solutions lower than 0.5%, by choosing the appropriate discretization (grid step). With increasing resolution, the simulation results converge to the analytical solution. Proper numerical convergence has been ascertained by varying the convergence criterium. The benchmark case tests the following fundamental solver features:

- that the EM LF Magneto Quasi-static Solver converges to the right solution
- that material interfaces are properly handled
- that the Biot-Savart sources are correctly implemented
- that post-processing correctly calculates derived quantities such as current density

The current density values at different positions inside the sphere match for the two methods with a deviation smaller than 0.5% for the finer discretization of the computational domain. With increasing resolution, the simulation results converge to the analytical solution.

Neither the spatial discretization nor the solution algorithm employed by Sim4Life and SEMCAD X use any assumptions based on the shape of the computational domain. This renders the approach suitable for any complex structures which might occur in biomedical applications. Because of this generalized verification approach it is valid to expect similarly accurate performance of the solver in simple geometries like the presented benchmarks and in more complex geometrical models.

In conclusion, the numerical MQS solver of Sim4Life and SEMCAD X therefore meets the requirements for modeling the magneto-quasistatic equation.

References

[1] J.R. Keltner. *Electromagnetic Fields of Surface Coil in Vivo NMR at High Frequencies, p.467-480, Magnetic Resonance in Medicine 22,* 1990.

[2] ZMT. *Sim4Life User Manual*, ZMT Zurich Med Tech, Zurich, Switzerland, 2015.